Inorganic Chemistry

Article

pubs.acs.org/IC

Fluorescence in Rhoda- and Iridacyclopentadienes Neglecting the Spin−Orbit Coupling of the Heavy Atom: The Ligand Dominates

Andreas Steffen,*[,†] Karine Costuas,*[,‡] Abdou Boucekkine,[‡] Marie-Hélène Thibault,[§] Andrew Beeby,[§] Andrei S. Batsanov,[§] Azzam Charaf-Eddin,[∥] Denis Jacquemin,[∥,⊥] Jean-François Halet,*[,‡] and Todd B. Marder*[,†,§]

[†]Institut für Anorganische Chemie, Universität Würzburg, Am Hubland, 97074 Würzburg, Germany

[‡]Institut des Sciences Chimiques de Rennes, UMR 6226 CNRS - Université de Rennes 1, 35042 Rennes Cedex, France

[§]Department of Chemistry, Durham University, South Road, Durham DH1 3LE, U.K.

[∥]CEISAM, UMR CNRS 6230, Université de Nantes, 2 rue de la Houssinière, 44322 Nantes Cedex 3, France

[⊥]Institut Universitaire de France, 103 bd Saint-Michel, 75005 Paris Cedex 05, France

Supporting Information

ABSTRACT: We present a detailed photophysical study and theoretical analysis of 2,5-bis(arylethynyl)rhodacyclopenta-2,4-dienes (**1a−c** and **2a−c**) and a 2,5-bis(arylethynyl)-iridacyclopenta-2,4-diene (**3**). Despite the presence of heavy atoms, these systems display unusually intense fluorescence from the S_1 excited state and no phosphorescence from T_1. The $S_1 \rightarrow T_1$ intersystem crossing (ISC) is remarkably slow with a rate constant of 10^8 s^{-1} (i.e., on the nanosecond time scale). Traditionally, for organometallic systems bearing 4d or 5d metals, ISC is 2−3 orders of magnitude faster. Emission lifetime measurements suggest that the title compounds undergo $S_1 \rightarrow T_1$ interconversion mainly via a thermally activated ISC channel above 233 K. The associated experimental activation energy is found to be $\Delta H^{\ddagger}_{ISC}$ = 28 kJ mol^{-1} (2340 cm^{-1}) for **1a**, which is supported by density functional theory (DFT) and time-dependent DFT calculations [$\Delta H^{\ddagger}_{ISC}$(calc.) = 11 kJ mol^{-1} (920 cm^{-1}) for **1a-H**]. However, below 233 K a second, temperature-independent ISC process via spin−orbit coupling occurs. The calculated lifetime for this $S_1 \rightarrow T_1$ ISC process is 1.1 s, indicating that although this is the main path for triplet state formation upon photoexcitation in common organometallic luminophores, it plays a minor role in our Rh compounds. Thus, the organic π-chromophore ligand seems to neglect the presence of the heavy rhodium or iridium atom, winning control over the excited-state photophysical behavior. This is attributed to a large energy separation of the ligand-centered highest occupied molecular orbital (HOMO) and lowest unoccupied MO (LUMO) from the metal-centered orbitals. The lowest excited states S_1 and T_1 arise exclusively from a HOMO-to-LUMO transition. The weak metal participation and the cumulenic distortion of the T_1 state associated with a large S_1−T_1 energy separation favor an "organic-like" photophysical behavior.

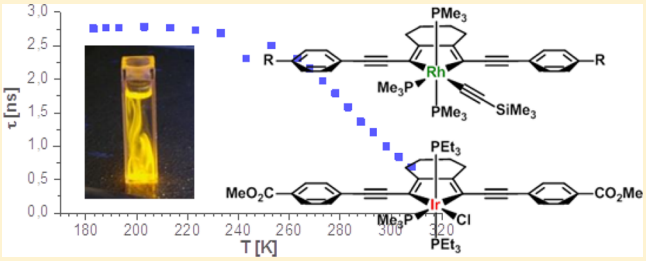

INTRODUCTION

Major developments have been achieved in recent years in applications of materials exhibiting long-lived excited triplet states, such as in organic light-emitting diodes (OLEDs),[1−6] light-harvesting antennas for solar cells,[7−12] and photocatalysis.[13−18] Research in these areas has mainly been stimulated by the fact that excited triplet states (T_n) exhibit different photophysical and photochemical properties compared with excited singlet states (S_n), such as longer lifetimes τ, lower-energy emission wavelength λ_{em}, different redox potentials E_{ox}/E_{red}, diradical character, etc.[19] $T_1 \rightarrow S_0$ emission (phosphorescence) is normally spin-forbidden if the spin−orbit coupling (SOC) between the two states is weak. This is generally the case in ordinary organic luminophores.[4,20] Thus, the S_1 state is formed according to Kasha's rule and tends to release its energy by $S_1 \rightarrow S_0$ emission (fluorescence), whereas the T_1 state, if generated at all, relaxes by the release of heat. However, efficient formation of the excited triplet states T_n and emission from them can be achieved by incorporation of a heavy atom into a rigid organic framework. Because of the non-negligible SOC effects, this leads to the partial breakdown of the spin selection rules that determine transitions between states. The rate of intersystem crossing (ISC) processes tends to scale with the spin−orbit coupling constant (ξ) of the heavy atom incorporated into the molecule, as observed, for example, for halogen-substituted naphthalenes.[21]

Organometallic complexes incorporating late transition metals have gained special attention for triplet state formation in photocatalysis and as phosphorescent materials. It soon became clear from the early works of Balzani and co-workers on the prototypical compound $[Ru(bpy)_3]^{2+}$ and its derivatives

Received: May 16, 2014
Published: June 12, 2014

   dx.doi.org/10.1021/ic501115k | Inorg. Chem. 2014, 53, 7055−7069

that the combination of heavy metals exhibiting exceptionally high intrinsic SOC with a variety of different ligands allows facile tuning of the excited states.[22,23] As a consequence, fast ISC occurs, quenching the fluorescence from S_1, and highly efficient radiative decay from the T_1 state (phosphorescence) with quantum yields (Φ_p) of up to unity can be observed.[19,24] A large number of phosphorescent transition-metal compounds mainly based on Ru (ξ = 1259 cm^{-1}), Re (ξ = 2200 cm^{-1}), Os (ξ = 3500 cm^{-1}), Ir (ξ = 3909 cm^{-1}), or Pt (ξ = 4000 cm^{-1}) with bipyridine, 2-phenylpyridine, phenyltriazolate, or phenyltetrazolate ligands have been synthesized.[1,2,10,17,23,25−29] Their excited states are usually described as metal-to-ligand charge transfer (MLCT), ligand-to-ligand charge transfer (LLCT), or intraligand charge transfer (ILCT) states or mixtures thereof. Only a few of those compounds show residual fluorescence (fluorescence quantum yield Φ_f < 1%), the low efficiency of which is attributed to the fast ISC.[25,30−33] In fact, ultrafast conversion of the S_1 state to the T_n states on the time scale of vibrations (i.e., a few femtoseconds) was found by the groups of Chergui and McCusker.[31,34−36] They carried out picosecond flash spectroscopy on bipyridyl complexes of Fe, Ru, and Re in order to elucidate the time dependence of the ISC processes on the nature of the transition metal present. Surprisingly, the iron and ruthenium bipyridyl complexes exhibited the fastest intersystem crossing (ca. 15 fs), although one would expect an opposite trend according to the SOC constants of the metal atoms (Re, ξ = 2200; Ru, ξ = 1259; Fe, ξ = 382 cm^{-1}). The authors explained this behavior by the geometric similarity of the ^{1}MLCT and ^{3}MLCT states, which, in addition to the already very strong coupling by spin−orbit interactions of the metal d electrons, can couple diabatically by high-frequency vibrations in a strongly non-Born−Oppenheimer regime.

Those recent results gave fresh impetus to the discussion of the importance of the "heavy atom effect" in such complexes, which questions the traditional picture of the physics of photoexcitation, according to which all steps [excitation, internal conversion (IC), ISC, emission] should be well-separated in time and energy (Figure 1).[20,37−40] It is of great importance to note that in the past few years, some reports have appeared addressing the opposite effect of unusually slow $S_n \rightarrow T_n$ ISC in organometallic compounds despite the presence of 4d and 5d transition-metal atoms.

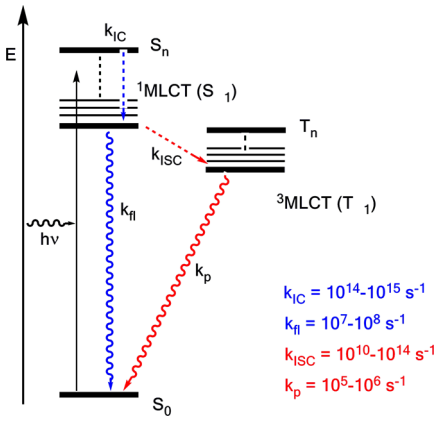

Figure 1. Simplified Jablonski diagram illustrating the fundamental processes and their typical rate constants in organometallic complexes after photoexcitation (f = fluorescence, p = phosphorescence, IC = internal conversion, ISC = intersystem crossing).

Unusually slow ISC leading to fluorescence (Φ_f = 0.22) has been observed in $[(TEE)\{AuPCy_3\}_4]$ (TEE = tetraethynylethene) despite the presence of four gold atoms, while $[\{TEB\}\{AuPCy_3\}_3]$ (TEB = 1,3,5-triethynylbenzene) with only three Au(I) ions displays phosphorescence (Φ_p = 0.46).[41−45] On the basis of time-dependent density functional theory (TD-DFT) calculations, Che and co-workers explained the behavior of these linear-coordinated Au(I) systems by the mutual cancellation of the SOC matrix elements of each Au atom in the Au_4 compound.[43]

We recently reported the synthesis and photophysical properties of 2,5-bis(arylethynyl)rhodacyclopenta-2,4-dienes, which exhibit fluorescence with quantum yields of up to Φ_f = 0.69 and no observed phosphorescence even at 77 K in a glass matrix.[46] A picosecond time-resolved IR spectroscopic investigation confirmed the slow formation of the T_1 state in nanoseconds instead of the fast ISC in femto- or picoseconds expected for octahedral organometallic complexes. To the best of our knowledge, this was the first reported example of such a slow ISC process in octahedral organometallic compounds.

In a series of oligothienylpyridine cyclometalated complexes of platinum and iridium, Kozhevnikov and co-workers observed fluorescence as well as phosphorescence.[47] Their interpretation was that the contribution of the metal character is still sufficient to promote phosphorescence but not large enough to induce the ultrafast depletion of the singlet state that normally occurs for complexes with discrete arylpyridine ligands. Similar behavior was found in Rh-based dipyrromethane complexes by Kirsch-De Mesmaeker and co-workers, who observed that at room temperature fluorescence originating from the ligand dominates, while at 77 K phosphorescence is the main process.[48]

Ligand-based fluorescence instead of the expected phosphorescence has also been reported for various fused aromatic systems (e.g., anthracene or pentacene) linked to a transition-metal atom via an alkynyl group or a keto group.[49−66] It has been suggested that acceleration of the $S_1 \rightarrow T_1$ ISC does not occur in this case because of the long distance between the metal atom and the ligand chromophore, diminishing the MLCT character and the influence of the metal in the excited states. An exceptional example is $[\{C_6H_3(CH_3)_2\}NCPt(PEt_3)_2]_2$-5,12-diethynyltetracene dication, which exhibits a fluorescence quantum yield of Φ_f = 0.97.[67]

All of these observations raise the question of the importance of the heavy atom effect with respect to structural and electronic parameters and the correlation with the formation of the triplet excited state and its emissive properties (i.e., phosphorescence). Herein we provide a detailed account, including temperature-dependent photophysical measurements and detailed DFT/TD-DFT analysis, of some representative examples of a series of 2,5-bis(arylethynyl)rhodacyclopenta-2,4-dienes and a related iridacyclopenta-2,4-diene to explain their unusual excited-state behavior, namely, exceptionally high fluorescence quantum yields (Φ_f = 0.33−0.69) with slow ISC and no observable phosphorescence at 77 K. We show that several factors, including the specific energies and nodal properties of the frontier orbitals in the ground states, structural changes in the excited states, and rigidity of the ligand, have to be taken into account to understand the role of the heavy atom in the ISC between S_1 and T_n and between T_1 and S_0. In the title metallacyclopentadiene series, a combination of those factors leads to small spin−orbit couplings regardless of the

dx.doi.org/10.1021/ic501115k | Inorg. Chem. 2014, 53, 7055−7069

Scheme 1. Synthesis of 2,5-Bis(*p*-R-arylethynyl)rhodacyclopenta-2,4-dienes 1a−c and 2a−c[46]

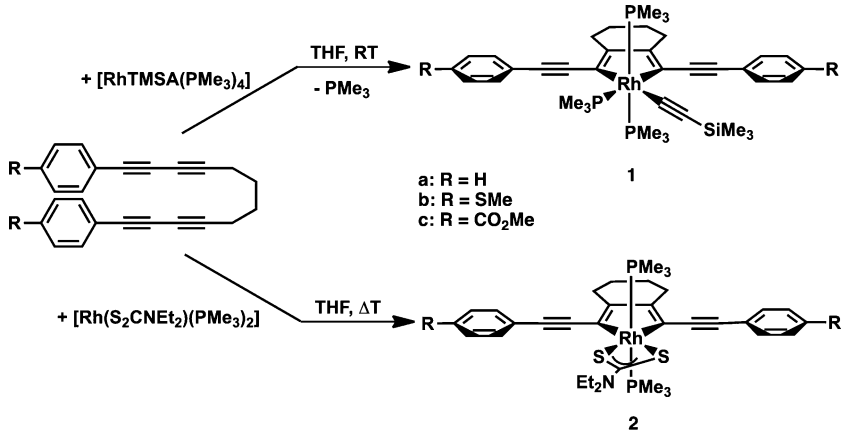

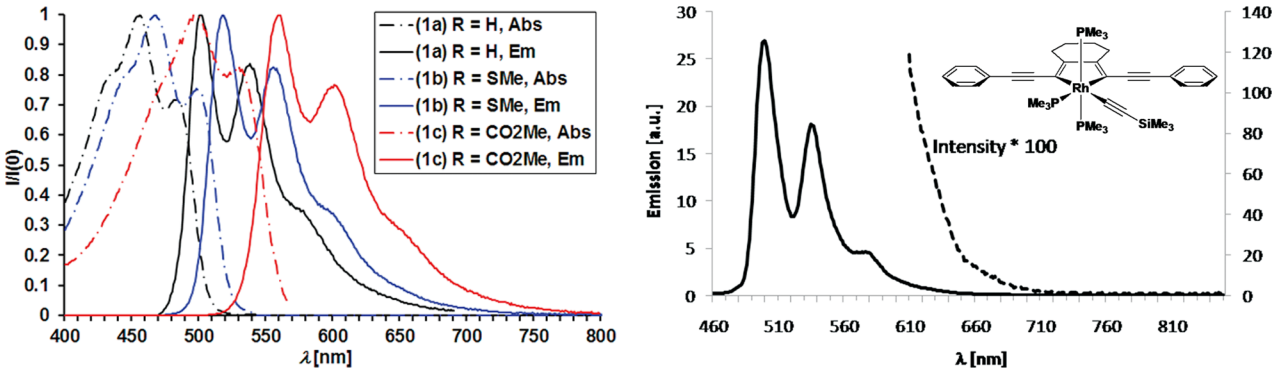

Figure 2. (left) Absorption spectra (dot-dashed lines) and emission spectra with excitation at the respective absorption maxima (solid lines) of **1a−c**. (right) Emission spectrum of **1a** at 77 K in an isopentane/Et_2O/EtOH glass matrix (λ_{ex} = 450 nm).[46]

Table 1. Selected Photophysical Properties of Rhodacyclopenta-2,4-dienes[46] 1a−c and 2a−c and Iridacyclopenta-2,4-diene 3 Measured in Degassed Toluene at Room Temperature

compd	λ_{max}^{abs} [nm]	ε [mol^{-1} cm^{-1} dm^3]	λ_{max}^{em} [nm]	Φ_f	τ_f^a [ns]	τ_0^b [ns]	Φ_Δ^c	k_f^d [10^8 s^{-1}]	k_Δ^e [10^8 s^{-1}]
1a	456	22000	501	0.33	1.2	3.6	0.65	2.75	5.42
1b	467	41000	518	0.34	1.8	5.3	0.40	1.89	2.22
1c	497	44000	560	0.69	3.0	4.3	0.26	2.30	0.87
2a	476	24000	526	0.07	1.0 (13%), 0.4 (87%)	6.8	0.32	1.47	
2b	487	21000	541	0.16	1.1 (72%), 0.7 (28%)	6.2	0.19	1.61	
2c	518	15000	586	0.46	2.5	5.4	0.20	1.84	0.80
3	515	21000	595	0.08	1.9 (41%), 0.9 (59%)	16.3	0.22	0.61	

[a]Observed fluorescence lifetime. [b]Intrinsic (pure radiative) lifetime (see eq 1). [c]Quantum yield for $^1O_2$ (Δ) formation in O_2-saturated solutions. [d]Rate constant for fluorescence. [e]Rate constant for Δ generation.

intrinsically large spin−orbit coupling constant of the metal atom involved.

RESULTS

Synthesis and Photophysical and Electrochemical Measurements. We previously described the synthesis of a series of 2,5-bis(*p*-R-arylethynyl)-3,4-bis(aryl)rhodacyclopenta-2,4-dienes by the remarkably regioselective reductive coupling of 1,4-bis(aryl)buta-1,3-diynes at Rh(I) precursors.[68,69] Intrigued by indications of unusual excited-state behavior in these complexes, we prepared more rigid derivatives (Scheme 1), which appeared to be surprisingly fluorescent from their S_1 states, as evidenced by their short emission lifetimes (τ_f = 1−3 ns) in degassed toluene solution at room temperature and by the overlap of their excitation and emission spectra (Figure 2 and Table 1).[46] The quantum yield for $^1O_2$ generation in an O_2-saturated solution was found to coincide with the $S_1 \rightarrow T_1$ ISC efficiency deduced from picosecond time-resolved transient IR measurements on **1a**, indicating that $^1O_2$ formation occurs only from the T_1 state of the rhodium complex. This assumption also appears reasonable because the intrinsic lifetime of S_1 is below 10 ns, the minimum lifetime for an excited state to be able to generate $^1O_2$ considering a diffusion rate constant of ca. 10^{10} dm^3 mol^{-1} s^{-1} and an O_2 concentration of ca. 10^{-3} mol dm^{-3}.

As the exceptionally high fluorescence quantum yields (Φ_f up to 0.69) and the quantum yields for $^1O_2$ formation in O_2-saturated solution (Φ_Δ) of the respective compounds sum to unity, one can conclude that the ISC also occurs on the nanosecond time scale, with very little to no nonradiative decay from S_1, and that the efficiency of $^1O_2$ formation from T_1 must be essentially 100%. An emission spectrum recorded at 77 K in

dx.doi.org/10.1021/ic501115k | Inorg. Chem. 2014, 53, 7055−7069

Scheme 2. Synthesis of 2,5-Bis(*p*-carbomethoxyphenylethynyl)iridacyclopentadiene 3

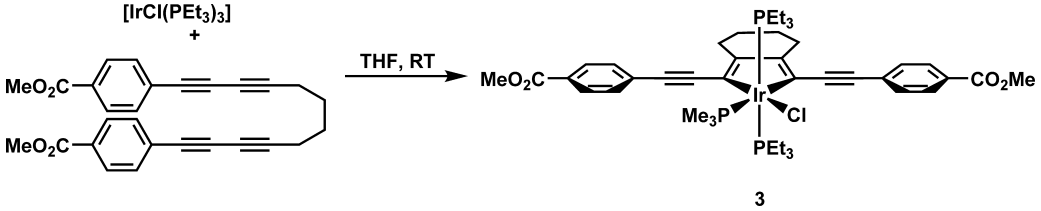

a glass matrix showed no additional bathochromically shifted phosphorescence between 400 and 1000 nm (Figure 2).

In order to elucidate the influence of the transition-metal center of the metallacyclopentadiene ring on the photophysical properties of the complexes, we also prepared an iridium analogue by the reaction of $[IrCl(PEt_3)_3]$ with 1,12-bis(*p*-carbomethoxyphenyl)dodeca-1,3,9,11-tetrayne (Scheme 2), as iridium complexes are very well known for their triplet emission and are the most widely employed class of organometallic phosphorescent materials in OLEDs.[1−5,27,70] The formation of the 2,5-bis(*p*-$MeO_2C-C_6H_4-C\equiv C$)iridacyclopenta-2,4-diene (**3**) occurred at room temperature after a few days, but the reaction rate could be increased by heating the THF solution to reflux. Interestingly, the formation of a π complex by coordination of the bis(diyne) occurs faster than the activation of the THF solvent by the Ir(I) fragment, a process that we reported to occur when PMe_3 instead of PEt_3 is used as a ligand in our studies concerning iridium-catalyzed nitrile hydration.[71] Complex **3** was unambiguously characterized by means of ^1H and ^{31}P NMR spectroscopy, mass spectrometry, and elemental analysis as well as X-ray diffraction studies of single crystals obtained from diffusion of hexane into a solution of **3** in chloroform (Figure 3).

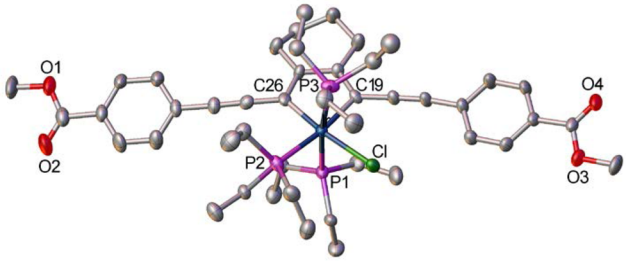

Figure 3. Molecular structure of **3** in the solid state as determined by single-crystal X-ray diffraction. Thermal ellipsoids are drawn at the 50% probability level, and the disorder of the ethyl groups and cyclohexyl ring and all of the H atoms have been omitted for clarity. Selected bond distances (Å): Ir−Cl 2.4662(16), Ir−P1 2.3616(12), Ir−P2 2.3891(15), Ir−P3 2.3693(13), Ir−C19 2.100(4), Ir−C26 2.028(4).

Compound **3** shows a poorly resolved low-energy absorption band in the visible region of the electromagnetic spectrum with λ_{max}^{abs} = 515 nm (ε = 21 000 M^{-1} cm^{-1}) and a broad emission with λ_{max}^{em} = 595 nm (Figure 4 and Table 1). Surprisingly, iridium complex **3** also displays fluorescence (Φ_f = 0.08) in deaerated toluene solution and no visible phosphorescence, a behavior not observed previously for luminescent iridium complexes. This is evidenced by the overlap of the absorption and emission bands as well as by the short luminescence lifetime [τ_f = 0.9 (59%)/1.9 (41%) ns], similar to that which was observed for the 2,5-bis(*p*-R-arylethynyl)rhodacyclopenta-2,4-dienes **1a−c** and **2a−c**, pointing again to an unusually slow

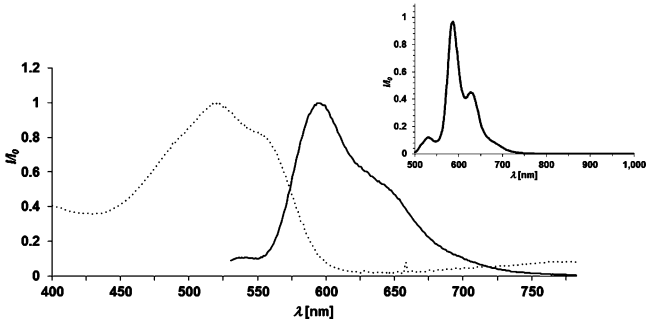

Figure 4. Absorption and emission spectra (λ_{ex} = 515 nm) of **3**. Inset: emission spectrum of **3** at 77 K in a glass matrix (λ_{ex} = 515 nm).

ISC process on the nanosecond time scale ($k_{ISC} = 10^8$ s^{-1}). An emission spectrum recorded at 77 K in a glass matrix (Figure 4 inset) showed a well-resolved emission band with an apparent vibrational progression of ca. 1020 cm^{-1}, but no phosphorescence in the range of 500−1000 nm was observed. Indirect measurements of the quantum yield for ISC by $^1O_2$ sensitization gave an estimated value of Φ_{ISC} = 0.22. However, it must be noted that **3** seems to be unstable in oxygen-saturated solutions under photolytic conditions.

The fact that emission occurs from the S_1 state in iridacyclopenta-2,4-diene **3** implies that the ISC processes are little-influenced or maybe even independent of the metal atom incorporated in the metallacycle, as the intrinsic spin−orbit coupling constant of Ir (ξ = 3909 cm^{-1}) is 3 times larger than that of Rh (1200 cm^{-1}). To the best of our knowledge, there is no other organometallic Ir system that exhibits fluorescence but not phosphorescence even at 77 K and has such slow ISC on the nanosecond time scale.

Compound **1a** was used as a model for further studies in order to rationalize the excited-state behavior of such conjugated, rodlike metallacyclopentadienes. This choice was driven by the fact that only two paths of deactivation were found experimentally: triplet state formation and single-exponential radiative decay ($\Phi_f + \Phi_\Delta \approx 1$; vide supra, Table 1). Measurement of the emission lifetime of **1a** at 77 K gave a value of τ_f = 3.2 ns, which is close to the calculated pure radiative lifetime of the first singlet excited state ($\tau_0 = \tau_f/\Phi_f$ = 3.6 ns; Table 1). This finding leads us to conclude that the ISC process occurs under thermal activation at room temperature and is inhibited at low temperatures. The temperature dependence of the conversion from the first singlet excited state to the triplet excited state T_1 was further probed by fluorescence lifetime measurements from room temperature down to 183 K in 5 K increments (Figure 5 and Table S1 in the Supporting Information). It can be seen from Figure 5 and eqs 1−3,

$$\tau_0 = \frac{\tau_f}{\Phi_f} \quad (1)$$

dx.doi.org/10.1021/ic501115k | Inorg. Chem. 2014, 53, 7055−7069

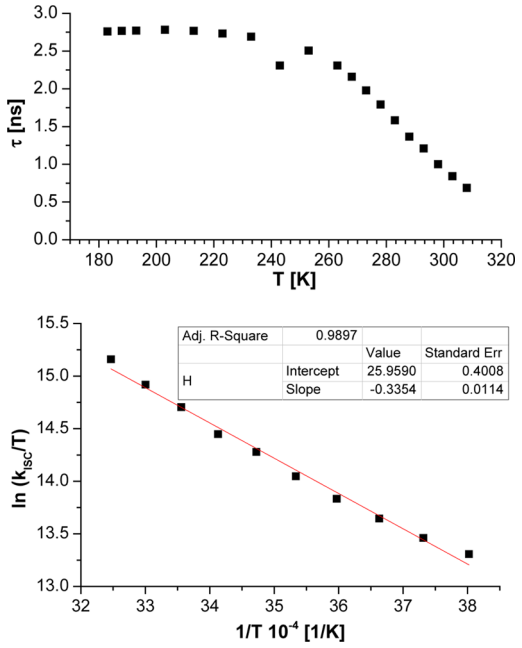

Figure 5. (top) Temperature-dependent emission lifetime measurements (λ_{ex} = 520 nm) in degassed toluene and (bottom) Eyring plot for **1a**.

$$\Phi_f = \frac{k_f}{k_f + k_{ISC}} \quad (2)$$

$$k_{ISC} = \frac{1 - \Phi_f}{\tau_f} = \frac{1}{\tau_f} - \frac{1}{\tau_0} \quad (3)$$

which are valid under the justified assumption that only radiative decay from S_1 to S_0 occurs (vide supra), that the emission lifetime τ_f and the fluorescence quantum yield Φ_f increase and thus the ISC rate constant (k_{ISC}) decreases gradually with decreasing temperature until T = 233 K, where a plateau is reached. The plateau ranging from 233 to 183 K indicates a constant Φ_f value of 0.77 in solution, and thus, the ISC does not seem to be completely shut off, although it is reduced to Φ_Δ = 0.23 (see eq 1 and Table 1). However, the ISC is further inhibited in an EPA glass matrix at 77 K, where an estimated Φ_f of 0.89 and an estimated Φ_Δ of 0.11 were observed. An Eyring plot [i.e., a plot of $\ln(k_{ISC}/T)$ vs $1/T$] over the temperature range 263−308 K, according to eqs 4 and 5,

$$k_{ISC} = \frac{k_B T}{h} e^{-\Delta H^{\ddagger}/RT} e^{\Delta S^{\ddagger}/R} \quad (4)$$

$$\ln \frac{k_{ISC}}{T} = -\frac{\Delta H^{\ddagger}}{R}\frac{1}{T} + \ln \frac{k_B}{h} + \frac{\Delta S^{\ddagger}}{R} \quad (5)$$

gives an activation enthalpy of $\Delta H^{\ddagger}_{ISC}$ = 28 kJ/mol (0.29 eV) for the ISC in toluene (Figure 5).

Cyclovoltammetry measurements were performed in acetonitrile versus $[FeCp^*_2]^{0/+}$ as the internal standard for the rhodacyclopentadienes **1a**−**c**, and the results are given in Table 2. All three compounds show fully reversible one-electron oxidation, which appears to be dependent on the para substituent of the phenyl rings, with the acceptor −CO_2Me (**1c**) having a larger effect than the donor −SMe (**1b**). A similar trend was observed in the red shift of the absorption and emission maxima of the respective compounds (see Figure 2).

Table 2. Cyclic Voltammetric and Spectroscopic Data for 1a−c and 2a

				E_{HOMO} [eV]	
compd	$E_{1/2}$ [V[a]]	λ^{abs}_{max} [nm]	λ^{em}_{max} [nm]	expt[b]	calc[c]
1a	0.354	456	501	−4.56	−4.43
1b	0.310	467	518	−4.52	−4.42
1c	0.461	497	560	−4.67	−4.71
2a	0.321	476	526	−4.53	−4.42

[a]All potentials are reported vs $[FeCp^*_2]/[FeCp^*_2]^+$ = 0.00 V and were obtained from 0.1 M nBu_4NPF_6/MeCN solutions at ambient temperature at a carbon working electrode. [b]$E_{HOMO} = -e[(E_{ox} - E_{1/2(Fc)}) + 4.8\ V]$. [c]Obtained from DFT calculations on model compounds (see the text and Figure 6).

The one-electron reduction wave lies outside the measurement window and thus was not recorded. With the assumption that the highest occupied molecular orbital (HOMO) energy of ferrocene lies 4.8 eV below vacuum,[72] the HOMO energies of **1a**−**c** can be estimated to be 4.56, 4.52, and 4.67 eV, respectively. Exchanging the PMe_3 and C≡C−$SiMe_3$ ligands in the equatorial plane of the metallacyclopentadiene ring in **1a** for a dithiocarbamate ligand in **2a** leads to a lower oxidation potential, indicating some metal contribution to the HOMO. The influence of the dithiocarbamate ligand on the oxidation potential and the HOMO energy compared with **1a** appears to be similar to the introduction of the −SMe substituent at the para position of the phenyl rings. However, this influence is small compared with the change in compound **1c**. Unfortunately, no data for the iridium complex **3** could be collected because it decomposed during the experiment. Nevertheless, the results are in agreement with previously collected data on related 2,5-bis(arylethynyl)-3,4-bis(aryl)rhodacyclopenta-2,4-dienes obtained by reductive coupling of 1,4-bis(aryl)-1,3-butadienes,[69] leading us to conclude that the HOMO is mainly located on the conjugated ligand system with little contribution from the metal.

DFT and TD-DFT Calculations. *Ground-State Properties and Vertical Franck−Condon Excitations.* In order to gain further insight into this exceptional excited-state behavior and to explain the observation of intense fluorescence rather than phosphorescence, we carried out DFT and TD-DFT studies on simplified derivatives of **1a**−**c** (exchange of $SiMe_3$ for H; **1a-H**−**1c-H**, respectively) and **3** (PMe_3 instead of PEt_3; **3-Me**) and on the original compound **2a**. Details of the calculations are given in Computational Details. The following discussion is mostly focused on *mer,cis*-[tris(trimethylphosphine)(ethynyl)-2,5-bis(phenylethynyl)cyclohexa[1′,2′:3,4]rhodacyclopenta-2,4-diene] (**1a-H**) (Scheme 3), as the parent compound **1a** was chosen for the temperature-dependent lifetime measurements. However, the general analysis applies equally to **1b-H**, **1c-H**, **2a**, and **3-Me** (also see the Supporting Information). DFT and TD-DFT calculations were performed to delineate the geometric and electronic structures of its ground state (S_0),

Scheme 3. Atom Numbering in 1a-H

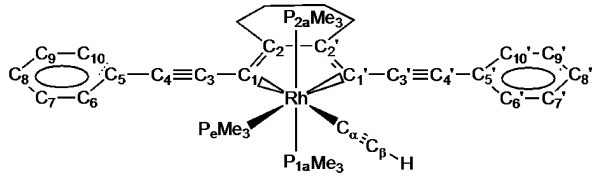

dx.doi.org/10.1021/ic501115k | Inorg. Chem. 2014, 53, 7055−7069

first singlet and triplet excited states (S_1 and T_1, respectively), and second triplet excited state (T_2).

The ground-state (S_0) geometry of **1a-H** was first optimized, and selected atomic separations are given in Table 3. A

Table 3. Selected Interatomic Distances (Å) of the Ground and Adiabatic Excited States of 1a-H

bond	expt[a]	S_0	S_1	T_1	T_2
Rh−P_e	2.3606(5)	2.424	2.440	2.429	2.425
Rh−P_{1a}	2.3160(5)	2.353	2.366	2.360	2.357
Rh−P_{2a}	2.3153(5)	2.354	2.366	2.360	2.357
Rh−C_α	2.0479(18)	2.039	2.043	2.038	2.036
C_α−C_β	1.218(2)	1.233	1.233	1.233	1.233
Rh−C_1	2.0993(17)	2.101	2.077	2.090	2.104
Rh−$C_{1'}$	2.0806(17)	2.073	2.057	2.062	2.075
C_1−C_2	1.374(2)	1.383	1.436	1.467	1.395
$C_{1'}$−$C_{2'}$	1.365(2)	1.378	1.430	1.460	1.390
C_2−$C_{2'}$	1.447(2)	1.447	1.399	1.371	1.466
C_1−C_3	1.419(2)	1.407	1.382	1.369	1.394
$C_{1'}$−$C_{3'}$	1.413(2)	1.404	1.377	1.367	1.390
C_3−C_4	1.205(3)	1.234	1.247	1.251	1.251
$C_{3'}$−$C_{4'}$	1.206(2)	1.230	1.243	1.246	1.249
C_4−C_5	1.435(3)	1.426	1.410	1.410	1.400
$C_{4'}$−$C_{5'}$	1.433(2)	1.424	1.409	1.410	1.395
C_5−C_6	1.401(3)	1.413	1.422	1.421	1.434
$C_{5'}$−$C_{6'}$	1.403(2)	1.413	1.421	1.420	1.437
C_6−C_7	1.383(3)	1.395	1.392	1.393	1.387
$C_{6'}$-$C_{7'}$	1.385(3)	1.395	1.392	1.392	1.386
C_7−C_8	1.384(3)	1.400	1.404	1.403	1.413
$C_{7'}$−$C_{8'}$	1.378(3)	1.401	1.404	1.403	1.414
C_8−C_9	1.384(3)	1.401	1.405	1.404	1.413
$C_{8'}$−$C_{9'}$	1.384(3)	1.401	1.404	1.403	1.414
C_9−C_{10}	1.388(3)	1.394	1.391	1.392	1.387
$C_{9'}$−$C_{10'}$	1.387(3)	1.395	1.392	1.393	1.386
C_{10}−C_5	1.403(3)	1.414	1.424	1.422	1.436
$C_{10'}$−$C_{5'}$	1.399(3)	1.412	1.421	1.419	1.436

[a]Obtained from single-crystal X-ray diffraction studies of 2,5-bis(phenylethynyl)rhodacyclopenta-2,4-diene **1a**.

comparison with the data experimentally determined by single-crystal X-ray diffraction studies of the 2,5-bis(phenylethynyl)-rhodacyclopenta-2,4-diene complex **1a** reveals that the metal−carbon and carbon−carbon separations are well-reproduced. However, the C≡C bond lengths are slightly overestimated by ca. 0.025 Å in the calculations, and as often seen in organometallic complexes, the DFT-computed values of the metal−phosphorus distances are somewhat overestimated with respect to the experimentally obtained separations, in this case by ca. 0.05 Å.[73,74]

The frontier orbital region of the molecular orbital (MO) diagram of **1a-H** is shown in Figure 6. The HOMO and lowest-unoccupied MO (LUMO) are well-separated in energy. In addition, they are somewhat isolated from the other occupied and vacant MOs by 1.36 and 1.14 eV, respectively. An analysis of their nodal properties indicates that they are π-type MOs, and they are heavily weighted on the organic π system of the conjugated ligand with very modest participation of the rhodium (ca. 4% in the HOMO and <2% in the LUMO) (Figure 7). The general trend of the relative HOMO energies as well as the small metal contribution are in agreement with the conclusions drawn from the cyclovoltammetry measurements (Table 2). The rhodium metal center lies in a pseudo-

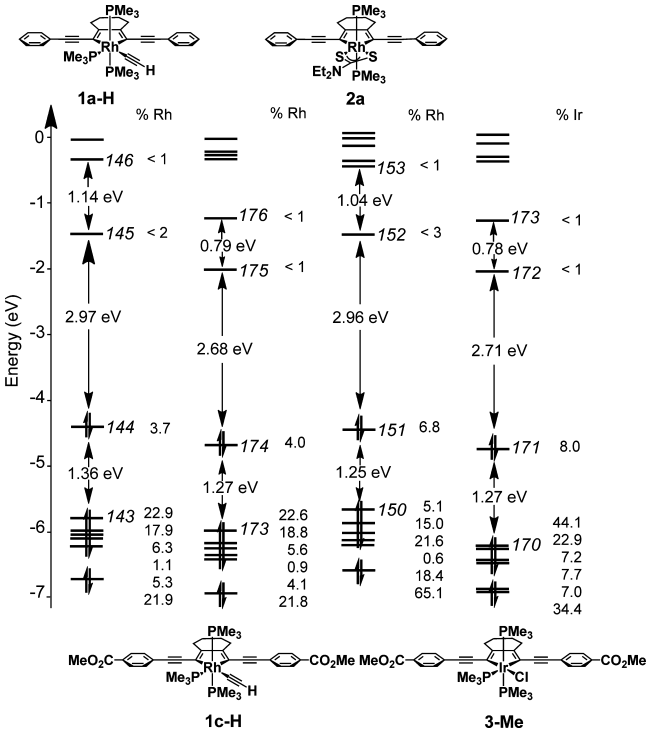

Figure 6. Molecular orbital diagrams of **1a-H**, **1c-H**, **2a**, and **3-Me**.

octahedral environment. Orbitals of "t_{2g}" and "e_g*" pseudosymmetry expected for octahedral ML_6 systems are found below the HOMO and above the LUMO, respectively. Introduction of the acceptor substituent −CO_2Me (**1c-H**) at the para position of the phenyl rings lowers the energy of the HOMO (a trend nicely reproduced by the cyclic voltammetry measurements), but its effect on the π* orbitals LUMO and LUMO+1 is greater, leading to a smaller HOMO−LUMO gap (Figure 6; also see the Supporting Information). Substitution of the PMe_3 and C≡C−$SiMe_3$ ligands in the equatorial plane by the electron-donating dithiocarbamate ligand changes the nature of the lower-lying occupied orbitals but leaves the frontier orbitals unaltered (compare **1a-H** and **2a** in Figure 6). Furthermore, although the substitution of iridium for rhodium does increase the metal d-orbital participation to ca. 8%, the frontier orbitals are still dominated by the ligand π system, as can be seen from a comparison of **1c-H** and **3-Me**.

One important question is the following: What makes the HOMO and the LUMO so energetically isolated from the other molecular orbitals? In comparison with a shorter and less π-conjugated ligand system such as a simple biphenylene, in the present case we have an extended and highly conjugated π system, namely, the bis(arylethynyl)butadiene backbone, with a small HOMO−LUMO gap. In addition, the strong ligand field gives rise to a large dπ−dσ* splitting. The small HOMO−LUMO gap of the π ligand and the large d-orbital splitting combine to disfavor interactions of the ligand-based orbitals with the metal d orbitals as a result of the increase in the energy difference and the decrease in overlap.

TD-DFT calculations were performed starting from the optimized S_0 ground-state structure in order to obtain the lowest excitation energies. First, vertical energies were calculated; solvent effects and geometric relaxation occurring after excitation were not considered. The resulting excited states thus represent the respective Franck−Condon (FC)

dx.doi.org/10.1021/ic501115k | Inorg. Chem. 2014, 53, 7055−7069

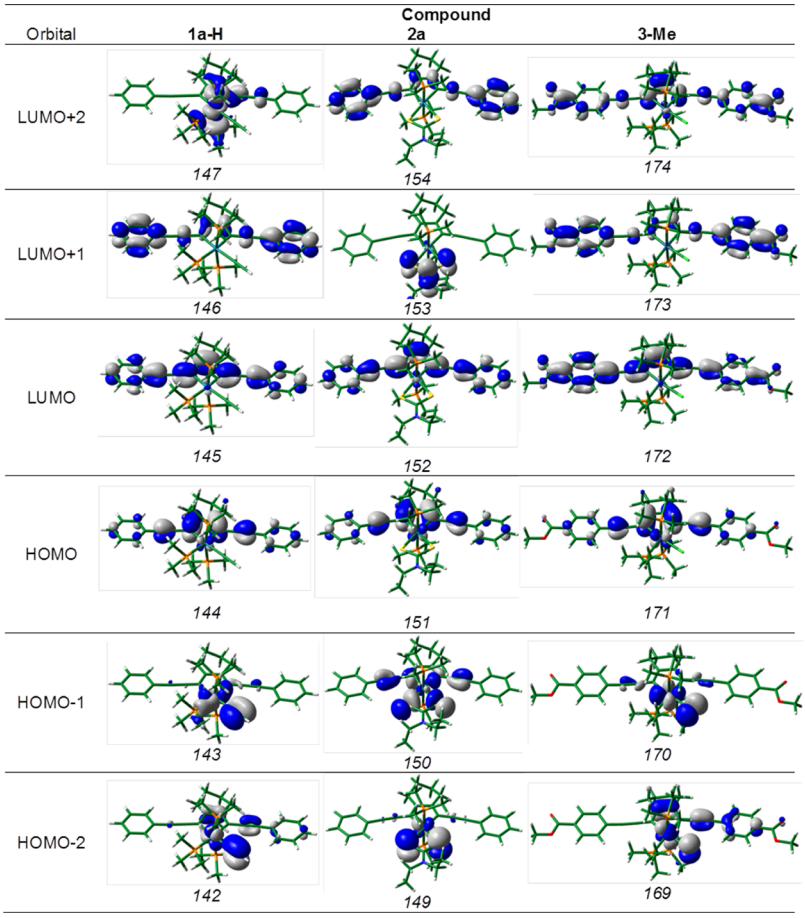

Figure 7. Isosurface plots of selected frontier molecular orbitals of **1a-H**, **2a**, and **3-Me**. Isocontour values: 0.035 $(e/bohr^3)^{1/2}$.

states in the gas phase. The excitation energies and main transitions (including their percentage contributions to the excitations) of **1a-H** are given in Figure 8 and Table 4. The lowest excited state is a triplet state (FC-T_1) with a calculated excitation energy of 1.06 eV. This would lead to phosphorescence in the near-IR (NIR) region (vide infra). It can be formally described as the result of an electronic transition from the HOMO to the LUMO. The second lowest excitation, with an oscillator strength of $f = 0.86$, leads to a singlet state (FC-S_1) with an associated energy of 2.50 eV. The third excited state (FC-T_2) is found at almost the same excitation energy (2.52 eV). The same situation arises by comparison of the FC-S_2 state, which is a result of a symmetry-forbidden HOMO → LUMO+2 transition ($f = 0.00$), and the FC-T_3 state, which are nearly degenerate at 3.11 and 3.09 eV, respectively.

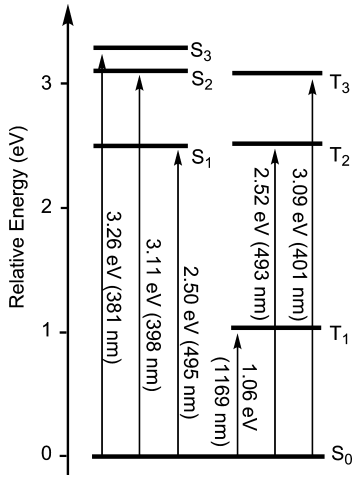

Figure 8. Jablonski diagram of the vertical electronic excitations (Franck–Condon states) of **1a-H** obtained by TD-DFT calculations.

The ground-state molecular orbital structure provides an explanation for the significant energy gap between the FC-S_1 and FC-T_1 states. As mentioned earlier, the HOMO and LUMO are both essentially ligand-based orbitals with π symmetry that are well-separated in energy from lower-lying filled orbitals with metal contribution. The first two excited states correspond to ligand-centered electronic transitions (π–π^*) (Table 3), as is common for fluorescent organic systems.[19,20] The large majority of organometallic compounds exhibit excited states with MLCT admixtures, which usually decrease the S_1–T_1 energy gap in comparison with that for local (π–π^*) excitation.[1,4,19,37,75]

The energy calculated for the FC first excited singlet state matches well with the first absorption peak found experimentally in toluene (λ_{max} = 456 nm, 2.72 eV), although solvent effects were not taken into account. A vibrational progression was proposed to interpret the rest of the experimental UV–vis absorption spectrum (i.e., the envelope of this large absorption band).[15] This assumption was based on a comparison with organic compounds incorporating aromatic rings, for which this type of vibronic structure can be observed. Indeed, our theoretical results on the FC states of **1a-H** reveal that the

dx.doi.org/10.1021/ic501115k | Inorg. Chem. 2014, 53, 7055–7069

Table 4. Vertical Electronic Excitation Energies and Main Transitions Describing the First Six Franck−Condon States of 1a-H Obtained by TD-DFT Calculations

excitation	energy [eV]	f	transition(s)[a]	configuration	classification[b]
$S_0 \rightarrow T_1$	1.06	–	HOMO → LUMO (99%)	$\pi-\pi^*$	^{3}IL
$S_0 \rightarrow S_1$	2.50	0.8559	HOMO → LUMO (98%)	$\pi-\pi^*$	^{1}IL
$S_0 \rightarrow T_2$	2.52	–	HOMO → LUMO+1 (49%)	$\pi-\pi^*$	^{3}IL/^{3}MLCT (19%)
			HOMO−4 → LUMO (26%)	$\pi-\pi^*$	
			HOMO−2 → LUMO (8%)	Rh-d/$\pi-\pi^*$	
$S_0 \rightarrow T_3$	3.09	–	HOMO → LUMO+2 (83%)	$\pi-\sigma^*$(Rh−P)	^{3}IL/^{3}LMCT (23%)
$S_0 \rightarrow S_2$	3.11	0.0000	HOMO → LUMO+2 (95%)	$\pi-\sigma^*$(Rh−P)	^{1}IL/^{1}LMCT (29%)
$S_0 \rightarrow S_3$	3.26	0.0004	HOMO−1 → LUMO (65%)	(Rh-d/TMS-π)−π^*	^{1}IL/^{1}MLCT (14%)
			HOMO−5 → LUMO (20%)	$\pi-\pi^*$	

[a]Only the major contributions are listed. [b]The percentage contributions of MLCT/LMCT are given in parentheses.

second singlet excited state (3.11 eV), which has negligible oscillator strength, cannot explain the shape of the absorption spectrum. In order to locate the vibronic states involved, we applied a computational protocol that allows simulation of the vibrational structure of absorption spectra (see Computational Details).[76,77] The harmonic vibrational frequencies of both states were computed on the respective optimized geometries using a method allowing accurate determination of vibronic couplings. The vibrationally resolved spectra were computed using the FC classes program taking into account solvent effects (see Computational Details).[78,79]

The computed vibrationally resolved absorption and emission spectra are compared with their experimental counterparts in Figure 9 (note that the emission has been

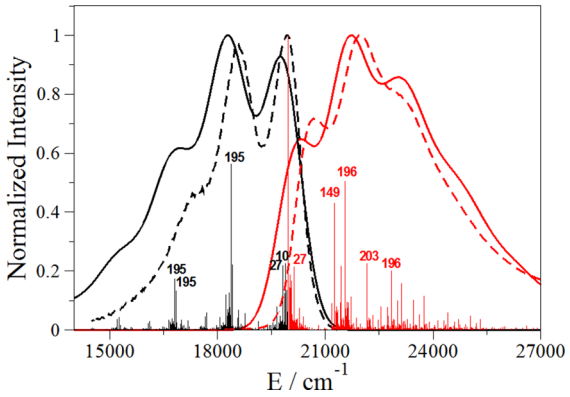

Figure 9. Vibrationally resolved absorption spectrum (black solid line) and emission spectrum (red solid line) computed at the M06-2X level. Both convoluted and stick spectra are shown, together with the numbering of the most important vibrational modes (given in the Supporting Information). The experimental absorption spectrum (black dashed line) and renormalized fluorescence spectrum (red dashed line) are given for comparison.

renormalized; see Computational Details). The good match with the experimental data is obvious: for absorption, a weaker band corresponding to the excitation between the lower-lying vibrational states (0−0) is present, followed by a second maximum and a shoulder; for emission, a structure with two maxima of similar intensities and a shoulder at longer wavelengths is found. The position of the 0−0 band, which includes vibrational zero-point energy (ZPE) corrections, is also in line with the experimental spectrum. This clearly confirms that the specific shapes of these bands are related to vibronic couplings and not to two (or more) energetically close electronically excited states. In Figure 9, the main vibrational modes contributing to both phenomena are given. Movies of these vibrational modes are available in the Supporting Information. For absorption (i.e., excited-state vibrations), modes 27, 149, 196, and 203 appear at 160, 1290, 1578, and 2191 cm^{-1}, respectively. The first mode corresponds to the deformation of the full molecule. The second and third modes can be mainly ascribed to the stretching of the double and single carbon−carbon bonds of the rhodacycle, respectively. Finally, mode 203 corresponds to stretching of the C≡C triple bonds attached to the central five-membered metallacycle. For emission, mode 27 (159 cm^{-1}) is similar to its excited-state counterpart, and the same holds for mode 195 (1585 cm^{-1}), which is localized on the central five-membered ring (as for mode 196 described above).

Excited-State Properties and ISC Processes. The geometries of the first excited singlet state S_1 and the first and second excited triplet states (T_1 and T_2) of **1a-H** were also optimized (Figure 10) using the same basis set and functional as for the ground state (see Computational Details). This allows direct comparisons with the previously discussed data. A comparison of the structural parameters is given in Table 3. The geometries of the optimized excited states differ significantly from that of the ground state, mainly in the rhodacyclopentadiene core and to a lesser extent in the 2,5-bis(phenylethynyl) moieties. Interestingly, calculated geometrical changes found for S_1 and T_1 show the same pattern. With reference to the ground-state S_0 geometry, the respective M−C, C═C, and C−C distances in the S_1 and T_1 states are overall up to a few of hundredths of an angstrom shorter, longer, and shorter, respectively, whereas the ethynyl C≡C distances are approximately 0.01 Å longer. In other words, the geometries of the S_1 and T_1 states develop some cumulenic character. This is in accordance with the nodal properties of the HOMO and LUMO in the S_0 state displayed in Figure 7, which would be depopulated and populated, respectively, in the excited states. Nevertheless, their geometries are different, particularly within the rhodacyclopentadiene core, where the double and single bond alternation, reversed compared with that in the S_0 state, is more marked in T_1 than in S_1 (1.467−1.371−1.460 vs 1.430−1.399−1.436 Å, respectively).

These geometrical differences can disfavor ISC from S_1 to T_1 considering their difference in energy (vide supra). Instead, we propose the thermal population of T_1 on the basis of the temperature-dependent emission lifetime for compound **1a** in toluene ($\Delta H^{\ddagger}_{ISC}$ = 0.29 eV) (vide supra). The activation barrier for **1a**-H was calculated to be $\Delta H^{\ddagger}_{ISC}$ = 0.11 eV via geometry optimization of the transition state between S_1 and T_1 (see

dx.doi.org/10.1021/ic501115k | Inorg. Chem. 2014, 53, 7055−7069

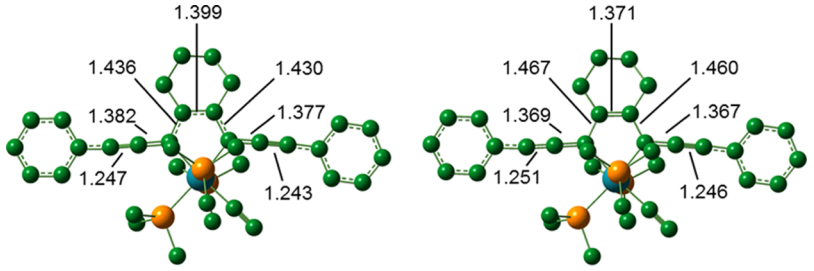

Figure 10. Calculated structures of **1a-H** in (left) the excited singlet state S_1 and (right) the excited triplet state T_1 (right). Hydrogen atoms have been omitted for clarity. Bond lengths are given in Å.

Computational Details), and this value is in good agreement with the experimental result. In addition, we searched for a transition state that could connect S_1 to T_2 because the FC-T_2 state is very close in energy to FC-S_1 (Table 4), making ISC from S_1 to T_2 a possible pathway. However, the resulting structure had the same geometry as the transition state found between S_1 and T_1. Thus, it is difficult to distinguish whether the system undergoes thermally activated ISC to T_1 or to T_2, but we can extrapolate that the energy of the transition state between S_1 and T_2 is at least that found for the thermal $S_1 \rightarrow T_1$ process. It is important to note that the spin density of the T_1 state is spread along the conjugated organic ligand system with very little rhodium contribution (less than 0.1 electron; see Figure 11), which must disfavor the emissive $T_1 \rightarrow S_0$ de-excitation (phosphorescence).

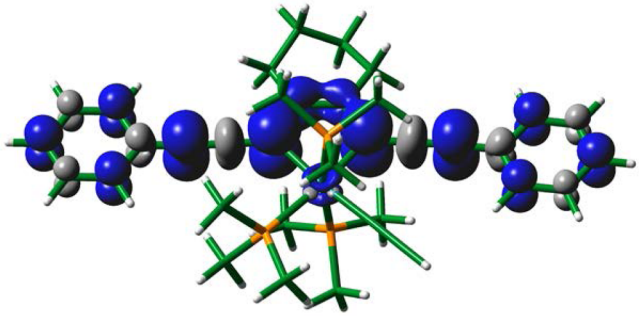

Figure 11. Spin density distribution of the optimized triplet excited state T_1 of **1a-H**. Isocontour values: 0.005 e/bohr^3.

In order to evaluate the intrinsic rate constants for the $S_1 \rightarrow T_1$ and $T_1 \rightarrow S_0$ vertical ISC processes, spin−orbit Tamm−Dancoff approximation (SO-TDA) TD-DFT calculations were performed (see Computational Details). The resulting calculated S_1 lifetime, for which no competitive emissive or nonradiative deactivation pathways were, of course, considered, was estimated to be 1.1 s. This was calculated via the Einstein coefficient of spontaneous emission. This value leads us to envisage the possibility that a thermal geometrical rearrangement occurs rather than direct ISC to T_1 (ps time scale). The same type of calculation revealed that the probability of ISC from T_1 to S_0 is also very low, with an estimated lifetime of 0.3 s. This time scale again allows nonradiative de-excitations to occur, which are particularly facile at low energy (above 1200 nm) according to the energy-gap law. Apart from our calculations on the T_1 state (Tables 4 and 5), which suggest a phosphorescence energy of ca. 1 eV (1240 nm), the quantitative sensitization of singlet oxygen from the triplet states of the rhodacyclopentadienes also leads us to expect a potential phosphorescence to occur within the above-mentioned wavelength range. This is due to the fact that $^1O_2$ emits at 1270 nm (0.98 eV), and therefore, the energy of the T_1 states of the rhodium compounds must be equal to or even higher than that value. We previously measured an emission spectrum in the range between 400 and 1000 nm. However, with our new knowledge of the energy of the T_1 state, we remeasured the spectrum of a degassed solution of **1a** in toluene in the region between 900 and 1400 nm at room temperature, where no phosphorescence could be detected. This new information is consistent with the calculated lifetime of 0.3 s for the phosphorescence, which allows for nonradiative decay by vibrational and/or rotational modes. Because only very little ISC occurred at 77 K in a glass matrix ($\Phi_\Delta \approx 0.1$; vide supra), we did not expect any emission to be observable within the instrument noise of the NIR photomultiplier tube at this temperature.

The vibrational frequencies were computed for each optimized state. Three vibrations were found between 1900 and 2200 cm^{-1} for **1a-H**, corresponding to vibrational modes involving the $C_3{\equiv}C_4$ and $C_{3'}{\equiv}C_{4'}$ stretching vibrators, coupled or not, and the $C_\alpha{\equiv}C_\beta$ (acetylide ligand) vibrator (Table 5). In each case, the most intense modes are different. For S_0, the $C_3{\equiv}C_4$ and $C_{3'}{\equiv}C_{4'}$ stretching vibrators are uncoupled and almost isoenergetic (2120 and 2146 cm^{-1}). For S_1 and T_1, the symmetric mode of the $C_3{\equiv}C_4/C_{3'}{\equiv}C_{4'}$ vibronic coupling is active (2005 and 1933 cm^{-1}, respectively). The energy difference is then explained by the change in the

Table 5. Relative ZPE-Corrected Energies ΔE (eV) and Calculated Frequencies (cm^{-1}),[a] Intensities (km·mol^{-1}, in Parentheses), and Natures of the C≡C Vibrational Modes for the Ground State and First Relaxed Excited States of 1a-H (See Scheme 3 for Atom Numbering)

state	ΔE	vibrational frequency (intensity) nature		
S_0	0.000	1949 (40) $C_\alpha{\equiv}C_\beta H$	2120 (513) $C_3{\equiv}C_4Ph$	2146 (287) $C_{3'}{\equiv}C_{4'}Ph$
T_1	0.985	1933 (445) $C_3{\equiv}C_4Ph + C_{3'}{\equiv}C_{4'}Ph$[b]	1950 (39) $C_\alpha{\equiv}C_\beta H$	1986 (2) $C_3{\equiv}C_4Ph - C_{3'}{\equiv}C_{4'}Ph$[c]
S_1	2.259	1948 (25) $C_\alpha{\equiv}C_\beta H$	2005 (836) $C_3{\equiv}C_4Ph + C_{3'}{\equiv}C_{4'}Ph$[b]	2057 (7) $C_3{\equiv}C_4Ph - C_{3'}{\equiv}C_{4'}Ph$[c]
T_2	1.339	1963 (845) $C_3{\equiv}C_4Ph + C_{3'}{\equiv}C_{4'}Ph$[b]	2049 (31) $C_\alpha{\equiv}C_\beta H$	2088 (3) $C_3{\equiv}C_4Ph - C_{3'}{\equiv}C_{4'}Ph$[c]

[a]A scaling factor of 0.9521 was applied to the vibrational frequencies.[80] [b]Symmetric vibration mode. [c]Asymmetric vibration mode.

dx.doi.org/10.1021/ic501115k | Inorg. Chem. 2014, 53, 7055−7069

C−C distances of the conjugated ligand in T_1 (see Table 3). These calculated results are in excellent agreement with the evolution of the time-resolved infrared (TRIR) vibrational absorption spectra, which we reported previously,[46] showing the disappearance of two bands at 2128 and 2142 cm^{-1} belonging to the ground state S_0. Immediately after photoexcitation, the appearance of a new band at 2008 cm^{-1} (S_1) is noted, and after 300 ps, a second band arises at 1942 cm^{-1} (T_1), growing with a time constant of $\tau \approx 1.6$ ns. The fact that T_2 (or another higher triplet excited state) was not noticeable in the TRIR experiments is most likely due to the expected short lifetimes of these states according to Kasha's rule.[19,20]

Similar theoretical analyses were also performed for rhodacyclopentadienes **1b-H**, **1c-H**, and **2a** and the new iridium compound **3-Me** (see the Supporting Information). All of them give a similar picture with the same conclusions as for the model compound **1a-H**.

DISCUSSION

The metallacyclopentadienes **1a−c**, **2a−c**, and **3** investigated here exhibit highly intense fluorescence from the S_1 state instead of phosphorescence at both room temperature and 77 K. The temperature-dependent emission lifetime measurements on **1a** (Figure 5) suggest that the $S_1 \rightarrow T_n$ ISC process is largely inhibited at low temperatures. We therefore conclude that a thermally activated ISC pathway exists with an activation barrier of $\Delta H^{\ddagger}_{ISC} = 28$ kJ mol^{-1} (0.29 eV) for **1a**. The energetic barriers for the ISC processes $S_1 \rightarrow T_1$ and $S_1 \rightarrow T_2$ in **1a-H**, which share the same transition state, were calculated by DFT methods to be on the same order of magnitude as the experimental value [i.e., $\Delta H^{\ddagger}_{ISC}$(calc.) = 11 kJ mol^{-1} (0.11 eV)], supporting this conclusion. In addition, for all of the compounds $^1O_2$ was shown to be formed in moderate yields in O_2-saturated solutions at room temperature (Table 1). Thus, the triplet state(s) is(are) formed on the nanosecond time scale ($k_{ISC} = 10^8$ s^{-1}) under these experimental conditions. The $S_1 \rightarrow T_1$ conversion occurs mainly by thermal activation from higher vibrational levels of the S_1 state or via a transition state (atomic motion), as shown in Scheme 4. Our experimental results reveal that the energy necessary for this structural change is not reached at 233 K. The even higher fluorescence efficiency of $\Phi_f = 0.89$ at 77 K (i.e., the lower ISC rate) could possibly be a result of the rigidity imposed by the glass matrix.

At first glance, this behavior is surprising, bearing in mind that ultrafast ISC channels due to the strong SOC mediated by the metal d electrons should be available to couple the singlet and triplet excited states, as has been found for the vast majority of Ru, Rh, Os, Re, Ir, and Pt complexes.[5,23,25−27,31,37] It should also be emphasized that although rhodium complexes are usually not very emissive in comparison to their iridium analogues, depletion of the S_1 state, which is mostly of $^1IL(\pi-\pi^*)$ character, via ISC to a triplet state is typically faster than fluorescence from S_1.[33,81−95]

SOC is often relatively small, especially in organic systems, and is often overlooked in quantum-chemical calculations. Nevertheless, it affects several physical phenomena such as ISC, for which the possibility of transitions between the involved states would be zero without the SOC component. ISC is emphasized, of course, when the difference in energy between the states is small but also when photoexcitation or emission involves strongly relativistic electrons (i.e., electrons surrounding heavy atoms). It is for this reason that the large majority of Ru, Os, Re, Ir, and Pt complexes are phosphorescent, as the absorption process has significant MLCT contributions (and the reverse for emission) involving d electrons.[5,23,25−27,31,37] Rhodium complexes are usually less emissive because of an important intraligand (IL) component in the excitation or emission processes that leads to weaker SOC than, for example, in iridium analogues, which show typical MLCT.[33,81−95]

Scheme 4. Summary of the Excited-State Processes upon Photoexcitation for 1a−c, 2a−c, and 3

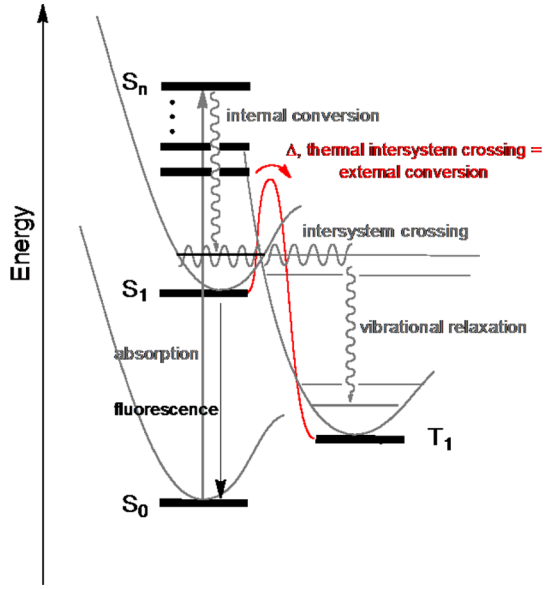

In the case of the metallacyclopentadienes **1a−c**, **2a−c**, and **3**, the "organic-like" photophysical behavior appears to be due to the electronic structure of the frontier orbitals, in which the HOMO and the LUMO are nearly pure ligand-type π and π^* orbitals, as confirmed by cyclic voltammetric measurements, and are well-separated from the lower- and higher-lying MOs, respectively (including metallic orbitals; vide supra). Consequently, the incorporation of Ir ($\xi = 3909$ cm^{-1}) in **3** instead of Rh ($\xi = 1200$ cm^{-1}) does not affect the composition of these frontier orbitals much (Figures 6 and 7) and does not significantly enhance the SOC component overlap between S_1 and T_1 or the interconversion rate (Table 1).

Two consequences arise from these findings that are confirmed by TD-DFT calculations: (1) electronic transitions originating from the frontier orbitals lead to the FC-S_1 and FC-T_1 states, which can be described as purely $^{1,3}IL(\pi-\pi^*)$ with presumably weak coupling, and (2) the relaxed S_1 and T_1 states are well-separated from excited states originating from transitions between lower occupied and higher unoccupied metal-based orbitals.

We also found that structural changes occur during the relaxation of T_1, which develops a more cumulenic character of the extended conjugated ligand in comparison to S_1, including important modifications of the bond distances in the rhodacyclopentadiene core (Table 3 and Figure 10). This fact, associated with more important electronic exchange energy in triplet states than in singlet states, leads to an energy difference of more than 1 eV between S_1 and T_1, hampering direct ISC between these two states. However, the proximity in energy and the similarity in structural arrangement of the S_1 and FC-T_2 states allows the possibility of an alternative ISC pathway. In that case, the participation of the metallic electrons in the excitation process would be small, definitely weaker than

dx.doi.org/10.1021/ic501115k | Inorg. Chem. 2014, 53, 7055−7069

that usually found in rhodium systems. Most probably, a thermal conversion to either T_2 or T_1 occurs (vide supra and Scheme 4). Thermally activated conversion does not rely on the presence of heavy atoms; indeed, it has been reported for organic perylene and anthracene derivatives.[96−99]

Our SO-TDA calculations suggest that the radiative $S_1 \rightarrow T_1$ ISC process occurs with a lifetime of 1.1 s, underlining the exceptionally weak coupling between these two states. Consequently, the emissive $T_1 \rightarrow S_0$ process has a calculated lifetime of ca. 0.3 s because of a weak SOC component in the overlap of its wave function with that of the FC singlet state FC-S_0 (almost-nonrelativistic electrons involved in the de-excitation process). It has to be noted also that the long intrinsic lifetime of T_1 allows for effective nonradiative decay by atomic motions and thus for geometry relaxation.

A comparison with other fluorescent organometallic systems incorporating heavy transition metals, such as rhodium, iridium, or platinum, shows the uniqueness of the 2,5-bis(arylethynyl)-metallacyclopentadienes. While mostly only residual fluorescence is observed,[25,30−33] more efficient fluorescence (i.e., slow ISC) is possible for chromophoric ligands to which a transition-metal center is linked, for example, via an alkynyl chain, as shown recently for dinuclear $[X(Et_3P)_2Pt]_2^{n+}$-5,12-diethynyltetracenes and -pentacenes (X = Cl, Br, I, $C{\equiv}CC_6H_5$, SC_6H_5, SeC_6H_5 for n = 0; X = PPh_3, PEt_3, NC_5H_5, $CN(Me)_2C_6H_3$ for n = 2).[55,67] However, the fact that the metal is linked instead of directly attached to the chromophore reduces the influence of the metal on the excited states. This increases the distance of the metal from the chromophore, leading to less SOC by the external heavy atom effect. A good, albeit very simplified, approximation for the efficiency of the SOC is given by the expression $k_{ISC} \propto Z^8/r^6$, where Z is the atomic number and r is the distance between the metal atom and the center of the chromophore involved in the transition.[100] The transition metal in our 2,5-bis(arylethynyl)metallacyclopenta-2,4-dienes **1a−c**, **2a−c**, and **3** is covalently bound directly to the center of the chromophoric ligand, but still does not participate in the transitions, leading to pure organic $^{1,3}IL(\pi-\pi^*)$ states as found for structurally related main-group 2,5-bis(arylethynyl)boroles, -siloles, -thiophenes, and -phospholes.[101−108]

CONCLUSION

The detailed photophysical and theoretical analysis of 2,5-bis(arylethynyl)rhodacyclopenta-2,4-dienes **1a−c** and **2a−c** and 2,5-bis(arylethynyl)iridacyclopenta-2,4-diene **3** carried out in this work provides a full picture of the excited-state behavior and clarifies the origin of the highly unusual slow intersystem crossing, which occurs with a rate constant of 10^8 s^{-1} (i.e., in nanoseconds). Normally, the intersystem crossing in 4d and 5d organometallic systems would be expected to be several orders of magnitude faster than the $S_1 \rightarrow S_0$ radiative decay. These compounds, which exhibit fluorescence ($S_1 \rightarrow S_0$ radiative decay) and no observable phosphorescence, undergo interconversion of their excited singlet state S_1 to the triplet state T_1 mainly via a thermally activated ISC channel above 233 K, for which we have determined the activation energy to be $\Delta H^{\ddagger}_{ISC}$ = 28 kJ mol^{-1} for **1a**, while only spin−orbit ISC occurs at lower temperatures. The general photophysical behavior of these octahedral compounds does not change dramatically upon substitution of the other ligands at the rhodium center or upon substitution of rhodium by iridium. The organic π-chromophore ligand apparently neglects the presence of the heavy rhodium or iridium atom, although they strongly covalently interact. DFT and TD-DFT studies revealed that the extended conjugation of the peculiar ligand causes the HOMO and LUMO to be ligand-centered π and π^* MOs that lie in between the metal-centered filled and vacant orbitals. The lowest excited states, S_1 and T_1, originate from electronic transitions between the HOMO and LUMO. This, in combination with a structural distortion to a cumulenic geometry in the excited T_1 state, leads to a weak coupling of the different spin states and thus to "organic-like" photophysical behavior.

Our results show that the ligand can win control over the photophysical excited-state behavior to such an extent that even heavy transition-metal atoms such as Rh or Ir participate in enhancing the fluorescence compared with their main-group analogues but basically do not influence the ISC processes. The awareness of the importance of the peculiar structure of the π-chromophoric ligand, such as the ones with extended conjugation used in this work, and the careful analysis of the spin−orbit interactions by the d electrons provide the possibility of other applications in the area of organometallic photophysics such as upconversion, nonlinear optics, NIR emitters, and even the use of first-row transition-metal centers for luminescent materials. This study sheds light on the true role of the heavy atom in excited-state processes that cannot be disassociated from its ligands. Further work to explore potential applications exploiting the combination of fluorescent "organic" behavior with "organometallic" triplet properties (such as $^1O_2$ sensitization) and stability is in progress.

EXPERIMENTAL SECTION

General Considerations. Unless otherwise stated, manipulations were performed using standard Schlenk or glovebox (Innovative Technology Inc.) techniques under an atmosphere of dry nitrogen (BOC). Reagent-grade solvents (Fisher Scientific and J.T. Baker) were nitrogen-saturated, dried and deoxygenated using an Innovative Technology Pure-Solv 400 solvent purification system, and further deoxygenated by the freeze−pump−thaw method. C_6D_6 and $CDCl_3$ were purchased from Cambridge Isotope Laboratories, dried over sodium/benzophenone and CaH_2, respectively, deoxygenated using the freeze−pump−thaw method, and vacuum-transferred into sealed vessels. The syntheses of the 2,5-bis(arylethynyl)rhodacyclopentadienes **1a−c** and **2a−c** have been reported previously.[46]

All of the NMR spectra were recorded at ambient temperature using a 400 MHz Varian Mercury spectrometer (^1H, 400 MHz; $^{13}C\{^1H\}$, 100 MHz; $^{31}P\{^1H\}$, 162 MHz). ^1H NMR chemical shifts are reported relative to tetramethylsilane (TMS) and were referenced to residual proton resonances of the corresponding deuterated solvent (C_6D_6, 7.16 ppm), whereas ^{13}C NMR spectra are reported relative to TMS using the carbon signals of the deuterated solvent (C_6D_6, 128.39 ppm). ^{31}P NMR spectra were referenced to external 85% H_3PO_4. Elemental analyses were obtained using an Exeter Analytical Inc. CE-440 elemental analyzer. Unit mass resolution spectrometric determinations were obtained using a MALDI ToF Applied Biosystems Voyager-DE STR mass spectrometer.

Cyclic voltammograms were recorded at v = 100 mV s^{-1} from 0.1 M $(^nBu)_4NPF_6$/MeCN solutions containing ca. 1×10^{-4} M analyte using a three-electrode cell equipped with a glassy carbon working electrode, Pt wire counter electrode, and Pt wire pseudoreference electrode. All of the redox potentials are reported with reference to an internal standard of the decamethylferrocene/decamethylferrocenium couple ($[FeCp^*_2]/[FeCp^*_2]^+$ = 0.00 V).

UV−vis absorption and emission spectra, lifetime, and quantum yield measurements were all recorded in degassed toluene. UV−vis absorption spectra and extinction coefficients were obtained on a Hewlett-Packard 8453 diode array spectrophotometer using standard 1 cm path length quartz cells. Fluorescence spectra and quantum yield measurements on dilute solutions with absorbance maxima of less than

dx.doi.org/10.1021/ic501115k | Inorg. Chem. 2014, 53, 7055−7069

0.2 were recorded on a HORIBA Jobin Yvon Fluoromax-3 spectrophotometer using the conventional 90° geometry. The emission spectra were fully corrected for the spectral response of the emission optical components using the manufacturer's correction curves. The quantum yield was measured using an integrating sphere with a HORIBA Jobin Yvon Fluorolog 3−22 Tau-3 spectrophotometer following a method described in the literature.[109] The absorbance of the samples was kept below 0.12 to avoid inner filter effects, and all of the measurements were carried out at room temperature.

The quantum yields of singlet oxygen formation were determined relative to perinaphthanone in toluene (Φ_Δ = 1.0) using a method described by Nonell and Braslavsky.[110] The samples and the reference compounds were analyzed in the same solvent because of the strong solvent dependence of the radiative and nonradiative rate constants for deactivation of the triplet states. The singlet oxygen emission was detected at 1269 nm from solutions in a 1 cm path length quartz cuvette after excitation at 355 nm using a frequency-tripled Q-switched Nd:YAG laser (Spectra Physics, Quanta Ray GCR-150-10) with a 10 Hz repetition rate. The emission was collected at 90° to the excitation beam using a liquid-nitrogen-cooled germanium photodiode (North Coast E0-817P) after passing through an interference filter centered at 1270 nm. The photodiode output was amplified and AC-coupled to a digital oscilloscope, which digitized and averaged the transients. The averaged data were then analyzed using the Microsoft Excel package.

The fluorescence lifetimes were measured via time-correlated single-photon counting (TCSPC) using a 396 nm pulsed laser diode. The fluorescence emission was collected at right angles to the excitation source; the emission wavelength was selected using a monochromator, and the emission was detected using a single-photon avalanche diode (SPAD). The instrument response function (IRF) was measured using a dilute LUDOX suspension as the scattering sample with the monochromator set at the emission wavelength of the laser, giving an IRF of 200 or 100 ps at 396 or 300 nm, respectively. The resulting intensity decay is a convolution of the fluorescence decay with the IRF, and iterative reconvolution of the IRF with the decay function and nonlinear least-squares analysis were used to analyze the convoluted data. Low-temperature emission spectra were recorded in an EPA glass at 77 K in a liquid-nitrogen-cooled Oxford Instruments OptistatDN cryostat. The same cryostat was used for the temperature-dependent lifetime measurements in degassed toluene.

Synthesis of *mer,cis*-[Tris(triethylphosphine)(chlorido)-2,5-bis(*p*-carbomethoxyphenylethynyl)cyclohexa[1′,2′:3,4]-iridacyclopenta-2,4-diene] (3). To a stirred solution of [IrCl-(PEt_3)$_3$] (50 mg, 0.086 mmol) in THF (5 mL) was added 1,12-bis(*p*-carbomethoxyphenyl)dodeca-1,3,9,11-tetrayne (36 mg, 0.086 mmol) dissolved in THF (5 mL) dropwise, and the reaction mixture was stirred overnight at room temperature. The volatiles were removed in vacuo. An NMR spectroscopic investigation showed complete conversion to **3**. The crude product was extracted with Et_2O and recrystallized several times from $CHCl_3$/hexane to obtain high-purity samples for photophysical studies and single crystals suitable for X-ray diffraction of **3**. Yield following purification: 61 mg (0.061 mmol, 71%).

Spectroscopic and analytical data: ^{1}H NMR (400 MHz, benzene-d_6, 25 °C, TMS): δ 8.11−7.86 (AA′XX′, 4H; CH_{arom}), 8.08−7.38 (AA′XX′, 4H; CH_{arom}), 3.44 (s, 3H; CO_2CH_3), 3.40 (s, 3H; CO_2CH_3), 3.03 (br m, 2H; CH_2), 2.85 (br m, 2H; CH_2), 2.28 (m, 6H; PCH_2), 2.10−1.80 (m, 12H; PCH_2), 1.65 (br m, 4H; CH_2), 1.08 (dt, ^3J(H,P) = 12 Hz, ^3J(H,H) = 8 Hz, 9H; PEt_3), 0.93 (vq, J = 7 Hz, 18H; PEt_3). ^{31}P{^{1}H} NMR (162 MHz) δ −31.9 (d, ^2J(P,P) = 19 Hz, 2P; PEt_3), −34.7 (t, ^2J(P,P) = 19 Hz, 1P; PEt_3). Anal. Calcd for $C_{46}H_{67}ClIrO_4P_3$: C, 55.00; H, 6.72. Found: C, 55.27; H, 6.68%. MS MALDI m/z = 1004 [M^+].

Single-crystal X-ray diffraction data were collected on a Bruker three-circle diffractometer with a SMART 6000 CCD area detector using graphite-monochromatized Mo Kα radiation (λ = 0.71073 Å); computations used SHELXTL-2013/2[111] and OLEX2[112] software. Crystal data: $C_{46}H_{67}ClIrO_4P_3$, M = 1004.56, T = 120 K, triclinic, space group $P\bar{1}$ (No. 2), a = 10.6570(13) Å, b = 12.9436(16) Å, c = 17.831(2) Å, α = 91.515(4)°, β = 95.930(4)°, γ = 107.886(4)°, V = 2302.5(8) Å^3, Z = 2, D_{calc} = 1.449 g cm^{-3}, μ = 3.10 mm^{-1}, 40 936 reflections with $2\theta \leq 60°$, 13 468 unique, R_{int} = 0.086, R_1 = 0.041 [10 430 data with $I \geq 2\sigma(I)$], $wR_2(F^2)$ = 0.095 (all data), CCDC-952768.

COMPUTATIONAL DETAILS

Some DFT calculations were carried out with the Gaussian 09 program,[113] including determination of the geometric structures, which were fully optimized without any symmetry constraints using the MPW1PW91 functional[114−116] with the LANL2DZ effective core potential basis set augmented by a polarization function for all atoms except hydrogens.[117] Harmonic vibrational frequency calculations were performed to check that the optimized geometries were energy minima and to compute ZPE corrections. The spin density isosurface representation was created using the GaussView 5.0 program.[118] The geometries and energies of the transition state between S_1 and T_1 and that between S_1 and T_2 were calculated using the geometries of T_1 and T_2, respectively, as the starting compounds and that of S_1 as the product by means of the synchronous transit-guided quasi-Newton method as implemented in Gaussian 09.[113,119] In both cases, two parallel calculations were performed with and without providing an initial geometry of the transition state (average of the main diverging distances and angles). The maximum sizes of the optimization steps were diminished to 0.005 Å and 0.6°. Those calculations were performed for the triplet spin state configuration, considering that the ISC occurs at fixed geometry. Vibrationally resolved absorption and emission spectra were calculated following a protocol detailed recently in the literature.[76,77] The ground- and excited-state structures were optimized using analytic DFT and TD-DFT gradients. These calculations were performed with the Gaussian 09.C01 program[113] using the M06-2X functional[120] and the 6-31G(d) atomic basis set. This choice was driven by the fact that the potential energy surfaces of excited states are different from their ground-state counterparts and necessitate the use of exchange−correlation functionals including a large share of *exact* exchange in order to avoid qualitative breakdowns (see refs 76 and 77 and references therein). The M06-2X/6-31G(d) combination is known to be valuable for TD-DFT calculations of 0−0 energies and band shapes.[76,77,121] To ensure numerically stable vibronic spectra, the force minimizations were performed until the residual mean square force was smaller than 1 × 10^{-5} a.u. The vibrationally resolved spectra within the harmonic approximation were computed using the FC Classes program.[78,79] The reported spectra were simulated using convoluted Gaussian functions presenting a full width at half-maximum (fwhm) of 0.07 eV. Maximal numbers of 25 overtones for each mode and 20 combination bands on each pair of modes were included in the calculations. The maximum number of integrals to be computed for each class was set to 1 × 10^{10}, and it was checked that such a number provided converged FC factors (>0.9; see the discussion in ref 76). In these calculations, the electrostatic interactions between the molecule and the environment (toluene) were modeled using the polarizable continuum model (PCM), which approximates solvent effects as long as no specific solute−solvent interactions take place.[122] In Figure 9, the experimental fluorescence spectrum measured on the wavelength scale was transformed in line shapes by applying an intensity correction proportional to ω^2, as this correction, which allows consistent theory/experiment comparisons, significantly affects the band shapes. DFT two-component SOC calculations were performed with the ADF2012.01 package.[123] For these calculations, the nonlocal MPW1PW91 corrections were added to the exchange and correlation energies, respectively. Calculations relying on the Tamm−Dancoff approximation (TDA) of the full TD-DFT equations were used to evaluate the lifetimes of the excited states and the oscillator strengths.[124]

ASSOCIATED CONTENT

Supporting Information

Temperature-dependent emission lifetime data for **1a**; further details of the DFT and TD-DFT results for **1a-H**, **1c-H**, **2a**, and **3-Me**, including Cartesian coordinates; X-ray crystallographic

dx.doi.org/10.1021/ic501115k | Inorg. Chem. 2014, 53, 7055−7069

data for **3** in CIF format; and movies (AVI) of the calculated main vibrational modes involved in the vibronic couplings in absorption and in emission of **1a-H**. This material is available free of charge via the Internet at http://pubs.acs.org.

AUTHOR INFORMATION

Corresponding Authors

*E-mail: andreas.steffen@uni-wuerzburg.de (A.S.).
*E-mail: kcostuas@univ-rennes1.fr (K.C.).
*E-mail: halet@univ-rennes1.fr (J.-F.H.).
*E-mail: todd.marder@uni-wuerzburg.de (T.B.M.).

Notes

The authors declare no competing financial interest.

ACKNOWLEDGMENTS

We acknowledge the very helpful comments of one of the anonymous reviewers, which further improved our work. A.S. thanks the DAAD and the EU (Marie-Curie FP-7) for postdoctoral fellowships. K.C., J.-F.H., and A. Boucekkine are grateful to the GENCI-CINES and GENCI-IDRIS for HPC resources (Grants 2012-80649 and 2013-80649). A.C.-E. thanks the European Research Council (ERC, Marches 278845) for his postdoctoral grant. D.J. acknowledges the European Research Council (ERC) and the Région des Pays de la Loire for financial support in the framework of a Starting Grant (Marches 278845) and a Recrutement sur Poste Stratégique, respectively. The vibronic calculations used resources of the GENCI-CINES/IDRIS (Grant c2012085117), Centre de Calcul Intensif des Pays de Loire (CCIPL), and a local Troy cluster. This work was supported by the Bavarian State Ministry of Science, Research, and the Arts for the Collaborative Research Network "Solar Technologies Go Hybrid". Part of this work was conducted within the scope of the CNRS Associated European Laboratory "Molecular Materials and Catalysis (MMC)" involving the Department of Chemistry of Durham University and the Institut des Sciences Chimiques de Rennes of the University of Rennes 1.

REFERENCES

(1) Yersin, H.; Rausch, A. F.; Czerwieniec, R.; Hofbeck, T.; Fischer, T. *Coord. Chem. Rev.* **2011**, *255*, 2622.
(2) Yersin, H. *Highly Efficient OLEDs with Phosphorescent Materials*; Wiley-VCH: Weinheim, Germany, 2008.
(3) Holder, E.; Langeveld, B. M. W.; Schubert, U. S. *Adv. Mater.* **2005**, *17*, 1109.
(4) Yersin, H. *Top. Curr. Chem.* **2004**, *241*, 1.
(5) Lamansky, S.; Djurovich, P.; Murphy, D.; Abdel-Razzaq, F.; Lee, H. E.; Adachi, C.; Burrows, P. E.; Forrest, S. R.; Thompson, M. E. *J. Am. Chem. Soc.* **2001**, *123*, 4304.
(6) Kalyanasundaram, K.; Grätzel, M. *Coord. Chem. Rev.* **1998**, *177*, 347.
(7) Wong, W. Y.; Ho, C. L. *Acc. Chem. Res.* **2010**, *43*, 1246.
(8) Grätzel, M. *Acc. Chem. Res.* **2009**, *42*, 1788.
(9) Robertson, N. *Angew. Chem., Int. Ed.* **2006**, *45*, 2338.
(10) Polo, A. S.; Itokazu, M. K.; Iha, N. Y. M. *Coord. Chem. Rev.* **2004**, *248*, 1343.
(11) Grätzel, M. *J. Photochem. Photobiol., C* **2003**, *4*, 145.
(12) Hagfeldt, A.; Grätzel, M. *Acc. Chem. Res.* **2000**, *33*, 269.
(13) Crabtree, R. H. *Organometallics* **2011**, *30*, 17.
(14) Bönnemann, H.; Khelashvili, G. *Appl. Organomet. Chem.* **2010**, *24*, 257.
(15) Morris, A. J.; Meyer, G. J.; Fujita, E. *Acc. Chem. Res.* **2009**, *42*, 1983.
(16) Arakawa, H.; Aresta, M.; Armor, J. N.; Barteau, M. A.; Beckman, E. J.; Bell, A. T.; Bercaw, J. E.; Creutz, C.; Dinjus, E.; Dixon, D. A.; Domen, K.; DuBois, D. L.; Eckert, J.; Fujita, E.; Gibson, D. H.; Goddard, W. A.; Goodman, D. W.; Keller, J.; Kubas, G. J.; Kung, H. H.; Lyons, J. E.; Manzer, L. E.; Marks, T. J.; Morokuma, K.; Nicholas, K. M.; Periana, R.; Que, L.; Rostrup-Nielson, J.; Sachtler, W. M. H.; Schmidt, L. D.; Sen, A.; Somorjai, G. A.; Stair, P. C.; Stults, B. R.; Tumas, W. *Chem. Rev.* **2001**, *101*, 953.
(17) Balzani, V.; Juris, A.; Venturi, M.; Campagna, S.; Serroni, S. *Chem. Rev.* **1996**, *96*, 759.
(18) Hawecker, J.; Lehn, J.-M.; Ziessel, R. *Helv. Chim. Acta* **1986**, *69*, 1990.
(19) Montalti, M.; Credi, A.; Prodi, L.; Gandolfi, M. T. *Handbook of Photochemistry*, 3rd ed.; CRC Press: Boca Raton, FL, 2006.
(20) Turro, N. J.; Ramamurthy, V.; Scaiano, J. C. *Photochem. Photobiol.* **2012**, *88*, 1033.
(21) Saigusa, H.; Azumi, T.; Sumitani, M.; Yoshihara, K. *J. Chem. Phys.* **1980**, *72*, 1713.
(22) Bomben, P. G.; Robson, K. C. D.; Koivisto, B. D.; Berlinguette, C. P. *Coord. Chem. Rev.* **2012**, *256*, 1438.
(23) Campagna, S.; Puntoriero, F.; Nastasi, F.; Bergamini, G.; Balzani, V. *Top. Curr. Chem.* **2007**, *280*, 117.
(24) Hedley, G. J.; Ruseckas, A.; Samuel, I. D. W. *J. Phys. Chem. A* **2009**, *113*, 2.
(25) Hsu, C. C.; Lin, C. C.; Chou, P. T.; Lai, C. H.; Hsu, C. W.; Lin, C. H.; Chi, Y. *J. Am. Chem. Soc.* **2012**, *134*, 7715.
(26) Kirgan, R. A.; Sullivan, B. P.; Rillema, D. P. *Top. Curr. Chem.* **2007**, *281*, 45.
(27) Flamigni, L.; Barbieri, A.; Sabatini, C.; Ventura, B.; Barigelletti, F. *Top. Curr. Chem.* **2007**, *281*, 143.
(28) Kaes, C.; Katz, A.; Hosseini, M. W. *Chem. Rev.* **2000**, *100*, 3553.
(29) You, Y.; Park, S. Y. *Dalton Trans.* **2009**, 1267.
(30) Buckner, S. W.; Fischer, M. J.; Jelliss, P. A.; Luo, R. S.; Minteer, S. D.; Rath, N. P.; Siemiarczuk, A. *Inorg. Chem.* **2006**, *45*, 7339.
(31) Cannizzo, A.; van Mourik, F.; Gawelda, W.; Zgrablic, G.; Bressler, C.; Chergui, M. *Angew. Chem., Int. Ed.* **2006**, *45*, 3174.
(32) Cheng, Y. M.; Yeh, Y. S.; Ho, M. L.; Chou, P. T.; Chen, P. S.; Chi, Y. *Inorg. Chem.* **2005**, *44*, 4594.
(33) Sexton, D. A.; Ford, P. C.; Magde, D. *J. Phys. Chem.* **1983**, *87*, 197.
(34) Cannizzo, A.; Blanco-Rodriguez, A. M.; El Nahhas, A.; Sebera, J.; Zalis, S.; Vlcek, A., Jr.; Chergui, M. *J. Am. Chem. Soc.* **2008**, *130*, 8967.
(35) Gawelda, W.; Cannizzo, A.; Pham, V.-T.; van Mourik, F.; Bressler, C.; Chergui, M. *J. Am. Chem. Soc.* **2007**, *129*, 8199.
(36) Monat, J. E.; McCusker, J. K. *J. Am. Chem. Soc.* **2000**, *122*, 4092.
(37) Chou, P. T.; Chi, Y.; Chung, M. W.; Lin, C. C. *Coord. Chem. Rev.* **2011**, *255*, 2653.
(38) Chergui, M. *Dalton Trans.* **2012**, *41*, 13022.
(39) Abedin-Siddique, Z.; Ohno, T.; Nozaki, K. *Inorg. Chem.* **2004**, *43*, 663.
(40) Abedin Siddique, Z.; Yamamoto, Y.; Ohno, T.; Nozaki, K. *Inorg. Chem.* **2003**, *42*, 6366.
(41) Ma, C. S.; Chan, C. T. L.; Kwok, W. M.; Che, C. M. *Chem. Sci.* **2012**, *3*, 1883.
(42) Lu, W.; Kwok, W. M.; Ma, C. S.; Chan, C. T. L.; Zhu, M. X.; Che, C. M. *J. Am. Chem. Soc.* **2011**, *133*, 14120.
(43) Tong, G. S. M.; Chow, P. K.; Che, C. M. *Angew. Chem., Int. Ed.* **2010**, *49*, 9206.
(44) Lu, W.; Zhu, N. Y.; Che, C. M. *J. Organomet. Chem.* **2003**, *670*, 11.
(45) Chao, H. Y.; Lu, W.; Li, Y. Q.; Chan, M. C. W.; Che, C. M.; Cheung, K. K.; Zhu, N. Y. *J. Am. Chem. Soc.* **2002**, *124*, 14696.
(46) Steffen, A.; Tay, M. G.; Batsanov, A. S.; Howard, J. A. K.; Beeby, A.; Vuong, K. Q.; Sun, X. Z.; George, M. W.; Marder, T. B. *Angew. Chem., Int. Ed.* **2010**, *49*, 2349.
(47) Kozhevnikov, D. N.; Kozhevnikov, V. N.; Shafikov, M. Z.; Prokhorov, A. M.; Bruce, D. W.; Williams, J. A. G. *Inorg. Chem.* **2011**, *50*, 3804.

(48) Ramlot, D.; Leen Volker, M. R.; Ovaere, M.; Beljonne, D.; Dehaen, W.; Van Meervelt, L.; Moucheron, C.; Kirsch-De Mesmaeker, A. *Eur. J. Inorg. Chem.* **2013**, 2031.
(49) Wilson, J. J.; Lippard, S. J. *Inorg. Chim. Acta* **2012**, *389*, 77.
(50) Prusakova, V.; McCusker, C. E.; Castellano, F. N. *Inorg. Chem.* **2012**, *51*, 8589.
(51) Zhao, G. J.; Yu, F. B.; Zhang, M. X.; Northrop, B. H.; Yang, H. B.; Han, K. L.; Stang, P. J. *J. Phys. Chem. A* **2011**, *115*, 6390.
(52) Zhang, B. G.; Li, Y. J.; Sun, W. F. *Eur. J. Inorg. Chem.* **2011**, 4964.
(53) Wu, W. T.; Wu, W. H.; Ji, S. M.; Guo, H. M.; Zhao, J. Z. *Dalton Trans.* **2011**, *40*, 5953.
(54) Wu, W. H.; Sun, J. F.; Ji, S. M.; Wu, W. T.; Zhao, J. Z.; Guo, H. M. *Dalton Trans.* **2011**, *40*, 11550.
(55) Nguyen, M. H.; Yip, J. H. K. *Organometallics* **2011**, *30*, 6383.
(56) Mancilha, F. S.; Barloy, L.; Rodembusch, F. S.; Dupont, J.; Pfeffer, M. *Dalton Trans.* **2011**, *40*, 10535.
(57) Lentijo, S.; Miguel, J. A.; Espinet, P. *Organometallics* **2011**, *30*, 1059.
(58) Nguyen, M. H.; Yip, J. H. K. *Organometallics* **2010**, *29*, 2422.
(59) Lentijo, S.; Miguel, J. A.; Espinet, P. *Inorg. Chem.* **2010**, *49*, 9169.
(60) Hudson, Z. M.; Zhao, S. B.; Wang, R. Y.; Wang, S. N. *Chem.—Eur. J.* **2009**, *15*, 6131.
(61) Lanoë, P.-H.; Fillaut, J.-L.; Toupet, L.; Williams, J. A. G.; Le Bozec, H.; Guerchais, V. *Chem. Commun.* **2008**, 4333.
(62) Khan, M. S.; Al-Mandhary, M. R. A.; Al-Suti, M. K.; Hisahm, A. K.; Raithby, P. R.; Ahrens, B.; Mahon, M. F.; Male, L.; Marseglia, E. A.; Tedesco, E.; Friend, R. H.; Köhler, A.; Feeder, N.; Teat, S. J. *J. Chem. Soc., Dalton Trans.* **2002**, 1358.
(63) Wilson, J. S.; Chawdhury, N.; Al-Mandhary, M. R. A.; Younus, M.; Khan, M. S.; Raithby, P. R.; Köhler, A.; Friend, R. H. *J. Am. Chem. Soc.* **2001**, *123*, 9412.
(64) Carano, M.; Cicogna, F.; Houben, J. L.; Ingrosso, G.; Marchetti, F.; Mottier, L.; Paolucci, F.; Pinzino, C.; Roffia, S. *Inorg. Chem.* **2002**, *41*, 3396.
(65) Cicogna, F.; Colonna, M.; Houben, J. L.; Ingrosso, G.; Marchetti, F. *J. Organomet. Chem.* **2000**, *593*, 251.
(66) Chen, Y. L.; Li, S. W.; Chi, Y.; Cheng, Y. M.; Pu, S. C.; Yeh, Y. S.; Chou, P. T. *ChemPhysChem* **2005**, *6*, 2012.
(67) Nguyen, M. H.; Wong, C. Y.; Yip, J. H. K. *Organometallics* **2013**, *32*, 1620.
(68) Rourke, J. P.; Batsanov, A. S.; Howard, J. A. K.; Marder, T. B. *Chem. Commun.* **2001**, 2626.
(69) Steffen, A.; Ward, R. M.; Tay, M. G.; Edkins, R. M.; Seeler, F.; van Leeuwen, M.; Pålsson, L.-O.; Beeby, A.; Batsanov, A. S.; Howard, J. A. K.; Marder, T. B. *Chem.—Eur. J.* **2014**, *20*, 3652.
(70) Adachi, C.; Baldo, M. A.; Thompson, M. E.; Forrest, S. R. *J. Appl. Phys.* **2001**, *90*, 5048.
(71) Crestani, M. G.; Steffen, A.; Kenwright, A. M.; Batsanov, A. S.; Howard, J. A. K.; Marder, T. B. *Organometallics* **2009**, *28*, 2904.
(72) Pommerehne, J.; Vestweber, H.; Guss, W.; Mahrt, R. F.; Bassler, H.; Porsch, M.; Daub, J. *Adv. Mater.* **1995**, *7*, 551.
(73) Dalton, D. M.; Rappe, A. K.; Rovis, T. *Chem. Sci.* **2013**, *4*, 2062.
(74) Barthes, C.; Lepetit, C.; Canac, Y.; Duhayon, C.; Zargarian, D.; Chauvin, R. *Inorg. Chem.* **2013**, *52*, 48.
(75) Rausch, A. F.; Homeier, H. H. H.; Yersin, H. *Top. Organomet. Chem.* **2010**, *29*, 193.
(76) Charaf-Eddin, A.; Planchat, A.; Mennucci, B.; Adamo, C.; Jacquemin, D. *J. Chem. Theory Comput.* **2013**, *9*, 2749.
(77) Jacquemin, D.; Planchat, A.; Adamo, C.; Mennucci, B. *J. Chem. Theory Comput.* **2012**, *8*, 2359.
(78) Santoro, F.; Lami, A.; Improta, R.; Barone, V. *J. Chem. Phys.* **2007**, *126*, No. 184102.
(79) Santoro, F.; Improta, R.; Lami, A.; Bloino, J.; Barone, V. *J. Chem. Phys.* **2007**, *126*, No. 084509.
(80) Yu, L.; Srinivas, G. N.; Schwartz, M. *J. Mol. Struct.: THEOCHEM* **2003**, *625*, 215.
(81) Lo, K. K. W.; Li, C. K.; Lau, K. W.; Zhu, N. Y. *Dalton Trans.* **2003**, 4682.
(82) Ghizdavu, L.; Lentzen, O.; Schumm, S.; Brodkorb, A.; Moucheron, C.; Kirsch-De Mesmaeker, A. *Inorg. Chem.* **2003**, *42*, 1935.
(83) Humbs, W.; Yersin, H. *Inorg. Chem.* **1996**, *35*, 2220.
(84) Calogero, G.; Giuffrida, G.; Serroni, S.; Ricevuto, V.; Campagna, S. *Inorg. Chem.* **1995**, *34*, 541.
(85) Colombo, M. G.; Brunold, T. C.; Riedener, T.; Güdel, H. U.; Förtsch, M.; Bürgi, H.-B. *Inorg. Chem.* **1994**, *33*, 545.
(86) Miki, H.; Shimada, M.; Azumi, T.; Brozik, J. A.; Crosby, G. A. *J. Phys. Chem.* **1993**, *97*, 11175.
(87) Zilian, A.; Gudel, H. U. *Inorg. Chem.* **1992**, *31*, 830.
(88) Milder, S. J.; Brunschwig, B. S. *J. Phys. Chem.* **1992**, *96*, 2189.
(89) van Diemen, J. H.; Haasnoot, J. G.; Hage, R.; Müller, E.; Reedijk, J. *Inorg. Chim. Acta* **1991**, *181*, 245.
(90) Barigelletti, F.; Sandrini, D.; Maestri, M.; Balzani, V.; von Zelewsky, A.; Chassot, L.; Jolliet, P.; Maeder, U. *Inorg. Chem.* **1988**, *27*, 3644.
(91) Maestri, M.; Sandrini, D.; Balzani, V.; Maeder, U.; von Zelewsky, A. *Inorg. Chem.* **1987**, *26*, 1323.
(92) Bergkamp, M. A.; Watts, R. J.; Ford, P. C.; Brannon, J.; Magde, D. *Chem. Phys. Lett.* **1978**, *59*, 125.
(93) Petersen, J. D.; Watts, R. J.; Ford, P. C. *J. Am. Chem. Soc.* **1976**, *98*, 3188.
(94) Halper, W.; Dearmond, M. K. *Chem. Phys. Lett.* **1974**, *24*, 114.
(95) Indelli, M. T.; Chiorboli, C.; Scandola, F. *Top. Curr. Chem.* **2007**, *280*, 215.
(96) Dreeskamp, H.; Koch, E.; Zander, M. *Chem. Phys. Lett.* **1975**, *31*, 251.
(97) Dreeskamp, H.; Koch, E.; Zander, M. *Ber. Bunsen-Ges. Phys. Chem.* **1974**, *78*, 1328.
(98) Bennett, R. G.; McCartin, P. J. *J. Chem. Phys.* **1966**, *44*, 1969.
(99) Ware, W. R.; Baldwin, B. A. *J. Chem. Phys.* **1965**, *43*, 1194.
(100) McGlynn, S. P.; Azumi, T.; Kinoshita, M. *Molecular Spectroscopy of the Triplet State*; Prentice Hall: Englewood Cliffs, NJ, 1969.
(101) Siddle, J. S.; Ward, R. M.; Collings, J. C.; Rutter, S. R.; Porres, L.; Applegarth, L.; Beeby, A.; Batsanov, A. S.; Thompson, A. L.; Howard, J. A. K.; Boucekkine, A.; Costuas, K.; Halet, J.-F.; Marder, T. B. *New J. Chem.* **2007**, *31*, 841.
(102) Baumgartner, T. *J. Inorg. Organomet. Polym.* **2005**, *15*, 389.
(103) Hissler, M.; Dyer, P. W.; Réau, R. *Coord. Chem. Rev.* **2003**, *244*, 1.
(104) Boydston, A. J.; Yin, Y.; Pagenkopf, B. L. *J. Am. Chem. Soc.* **2004**, *126*, 3724.
(105) Yamaguchi, S.; Tamao, K. *J. Organomet. Chem.* **2002**, *653*, 223.
(106) Steffen, A.; Ward, R. M.; Jones, W. D.; Marder, T. B. *Coord. Chem. Rev.* **2010**, *254*, 1950.
(107) Matano, Y.; Nakashima, M.; Imahori, H. *Angew. Chem., Int. Ed.* **2009**, *48*, 4002.
(108) Hay, C.; Hissler, M.; Fischmeister, C.; Rault-Berthelot, J.; Toupet, L.; Nyulászi, L.; Réau, R. *Chem.—Eur. J.* **2001**, *7*, 4222.
(109) Porrès, L.; Holland, A.; Pålsson, L.-O.; Monkman, A. P.; Kemp, C.; Beeby, A. *J. Fluoresc.* **2006**, *16*, 267.
(110) Nonell, S.; Braslavsky, S. L. *Methods Enzymol.* **2000**, *319*, 37.
(111) Sheldrick, G. M. *Acta Crystallogr.* **2008**, *A64*, 112.
(112) Dolomanov, O. V.; Bourhis, L. J.; Gildea, R. J.; Howard, J. A. K.; Puschmann, H. *J. Appl. Crystallogr.* **2009**, *42*, 339.
(113) Frisch, M. J.; Trucks, G. W.; Schlegel, H. B.; Scuseria, G. E.; Robb, M. A.; Cheeseman, J. R.; Scalmani, G.; Barone, V.; Mennucci, B.; Petersson, G. A.; Nakatsuji, H.; Caricato, M.; Li, X.; Hratchian, H. P.; Izmaylov, A. F.; Bloino, J.; Zheng, G.; Sonnenberg, J. L.; Hada, M.; Ehara, M.; Toyota, K.; Fukuda, R.; Hasegawa, J.; Ishida, M.; Nakajima, T.; Honda, Y.; Kitao, O.; Nakai, H.; Vreven, T.; Montgomery, J. A., Jr.; Peralta, J. E.; Ogliaro, F.; Bearpark, M.; Heyd, J. J.; Brothers, E.; Kudin, K. N.; Staroverov, V. N.; Kobayashi, R.; Normand, J.; Raghavachari, K.; Rendell, A.; Burant, J. C.; Iyengar, S. S.; Tomasi, J.; Cossi, M.; Rega, N.; Millam, N. J.; Klene, M.; Knox, J. E.; Cross, J. B.; Bakken, V.;

Adamo, C.; Jaramillo, J.; Gomperts, R.; Stratmann, R. E.; Yazyev, O.; Austin, A. J.; Cammi, R.; Pomelli, C.; Ochterski, J. W.; Martin, R. L.; Morokuma, K.; Zakrzewski, V. G.; Voth, G. A.; Salvador, P.; Dannenberg, J. J.; Dapprich, S.; Daniels, A. D.; Farkas, Ö.; Foresman, J. B.; Ortiz, J. V.; Cioslowski, J.; Fox, D. J. *Gaussian 09*, revisions A.02 and C.01; Gaussian, Inc.: Wallingford, CT, 2009.
(114) Adamo, C.; Barone, V. *J. Chem. Phys.* **1998**, *108*, 664.
(115) Perdew, J. P.; Burke, K.; Wang, Y. *Phys. Rev. B* **1996**, *54*, 16533.
(116) Perdew, J. P.; Burke, K.; Ernzerhof, M. *Phys. Rev. Lett.* **1996**, *77*, 3865.
(117) Hay, P. J.; Wadt, W. R. *J. Chem. Phys.* **1985**, *82*, 270.
(118) Varetto, U.; Giuffreda, M. G.; Jang, Y. *Abstr. Pap.—Am. Chem. Soc.* **2009**, *238*, COMP 151.
(119) Peng, C.; Schlegel, H. B. *Isr. J. Chem.* **1993**, *33*, 449.
(120) Zhao, Y.; Truhlar, D. G. *Theor. Chem. Acc.* **2008**, *120*, 215.
(121) Isegawa, M.; Peverati, R.; Truhlar, D. G. *J. Chem. Phys.* **2012**, *137*, No. 244104.
(122) Tomasi, J.; Mennucci, B.; Cammi, R. *Chem. Rev.* **2005**, *105*, 2999.
(123) te Velde, G.; Bickelhaupt, F. M.; Baerends, E. J.; Guerra, C. F.; Van Gisbergen, S. J. A.; Snijders, J. G.; Ziegler, T. *J. Comput. Chem.* **2001**, *22*, 931.
(124) Hirata, S.; Head-Gordon, M. *Chem. Phys. Lett.* **1999**, *314*, 291.